Investigating the plasma chemistry for the synthesis of carbon nanotubes/nanofibres in an inductively coupled plasma enhanced CVD system: the effect of different gas mixtures

M Mao, A Bogaerts

Investigating the plasma chemistry for the synthesis of carbon nanotubes/nanofibers in an inductively coupled plasma enhanced CVD system: Effect of different gas mixtures

M Mao, A Bogaerts

Research Group PLASMANT, Dept. of Chemistry, University of Antwerp, Universiteitsplein 1, B-2610 Antwerp, Belgium

Email: ming.mao@ua.ac.be

Abstract. A hybrid model, called the Hybrid Plasma Equipment Model (HPEM) was used to study an inductively coupled plasma in gas mixtures of H_2 or NH_3 with CH_4 or C_2H_2 used for the synthesis of carbon nanotubes or carbon nanofibers (CNTs/CNFs). The plasma properties are discussed for the different gas mixture at low and moderate pressure, and the growth precursors for CNTs/CNFs are analyzed. It is found that C_2H_2, C_2H_4, and C_2H_6 are the predominant molecules in CH_4 containing plasmas beside the feedstock gas, and serve as carbon sources for CNT/CNF formation. On the other hand, long chain hydrocarbons are observed in C_2H_2 containing plasmas. Furthermore, the background gases CH_4 and C_2H_2 show a different decomposition rate with H_2 or NH_3 addition at moderate pressures.

1. Introduction

Carbon nanotubes (CNTs) were first discovered by Iijima, in 1991 when he synthesized fullerenes (C_{60}) in an arc discharge reactor[1]. Since then CNTs gained a lot of attention due to their unique physical, chemical and electronic properties, as well as their wide potential applications including nanoelectronics[2], hydrogen storage[3], and field emission devices[4]. Carbon nanobutes are divided into two categories due to their different structures[5]: single-walled carbon nanotubes (SWCNTs) and multi-walled carbon nanotubes (MWCNTs). Special structures of MWCNTs are the multi-walled carbon nanofibers (MWCNFs) where the angle between the graphite basal planes and the tube axis is nonzero.

Several methods can be used for the synthesis of CNTs/CNFs, such as arc discharges[6], laser ablation[7], thermal chemical vapour deposition[8], and plasma enhanced chemical vapour deposition (PECVD)[9-31]. Among these growth techniques, PECVD has become a very promising technology for the direct synthesis of vertically aligned CNTs/CNFs used for field emission devices[32-35]. A variety of plasma sources, such as microwave discharges(MW)[9, 10], hot-filament(HF)[11], dc-glow discharges(DC)[12-14, 26, 27], RF capacitively coupled plasmas(CCP)[15, 16] and RF inductively coupled plasmas(ICP)[17-24, 30, 31], have been used to generate a plasma of typical feedstock mixtures such as CH_4 or C_2H_2 mixed with either H_2 or NH_3. The recent progress in PECVD for CNT/CNF synthesis has been summarized in table 1 and 2.

Cui *et al.*[9] used a microwave CH_4/NH_3 plasma and showed that aligned bamboo-like CNTs were deposited under their conditions. The effects of growth temperature and gas phase chemistry variations on the nanotube nucleation and growth structures were investigated. Their results indicated that both substrate temperature and carbon concentration in the gas phase had significant effects on the microstructure of aligned multi-walled tubes. Another demonstration on growing aligned CNTs in microwave C_2H_2/NH_3 plasma was reported by Bower *et al.*[10]. The alignment mechanism was studied in their paper. It was shown that the electrical self-bias

field imposed on the substrate surface from the plasma environment enabled a vertically oriented growth of MWCNTs.
Optical emission spectroscopy studies were performed by Gulas[11] in a plasma-enhanced hot filament CVD system for CNT growth for comparison with kinetic simulations of the plasma. They found that the formation of CN and HCN species significantly changed the density and morphology of the CNTs when NH_3 was diluted to the C_2H_2 plasma.
Chhowalla *et al.*[12] explored the growth process conditions for vertically aligned CNTs by dc-PECVD. The influence of the Ni catalyst dimensions, bias voltage, deposition temperature, C_2H_2:NH_3 ratio and pressure on the formation of the CNTs was studied. They showed that nanotube growth occurred by diffusion of carbon through the Ni catalyst particle, which moved up to the nanotube tip. The plasma composition of a dc C_2H_2/NH_3 plasma used for growing vertically aligned CNTs was analyzed by Bell *et al.*[13] by mass spectrometry. H_2, N_2 and HCN were found as the major neutral species beside C_2H_2 and NH_3. The dominant detected ions were NH_3^+ and $C_2H_2^+$, besides NH_2^+, NH_4^+, HCN^+ and C_2H^+. The role of NH_3 in CNT growth was investigated in their work. They found that NH_3 had two key roles in the CNT formation: generating atomic hydrogen to remove excess carbon and suppressing the decomposition of acetylene. An optimum C_2H_2/NH_3 gas ratio of around 20/80 was determined in the experiment giving rise to a minimum in H_2 density. Hofmann *et al.*[14] have successfully grown vertically aligned CNFs at a temperature as low as 120 °C using a dc-PECVD system. A systematic study of the temperature dependence of the growth rate indicated a lower activation energy of 0.23 eV in the PECVD system than in the thermal CVD system (1.2-1.5eV). They suggested that the diffusion of carbon on the catalyst surface is the rate-determining step at low temperature.
Okita *et al.*[15] investigated the effects of hydrogen on CNT formation in a capacitive CH_4/H_2 plasma in the pressure range of 1~10 Torr, a total flow rate of 30 sccm, 4 W input power and a growth time of 10~90 minutes. They concluded that the gas ratio of CH_4/H_2 = 27/3 at a growth time of 10 minutes was efficient for CNT growth, and the amount of carbon atoms in the CNT agreed well with results from 1D fluid simulations (see below). The hydrogen etching effect on CNTs was also studied by performing H_2 plasma treatment on as-grown CNTs. Their results indicated that MWCNTs were not etched by the H_2 plasma. Two-dimensional carbon nanowalls were deposited in CCP-PECVD with $C_2F_6(CH_4/CF_4)/H_2$ mixtures by Hiramatsu *et al.*[16]. Indeed, the authors found that the carbon nanowalls grown using CH_4/H_2 were waved and thin instead of vertically aligned.

The plasma most often used in the literature for CNT/CNF growth is the ICP. Delzeit and co-workers[17] carried out a study of growing MWCNTs on silicon substrates with multilayered Al/Fe catalysts in an inductively coupled CH_4/H_2 plasma. A detailed parametric study was undertaken by varying the inductive power, pressure, temperature, gas composition, catalyst thickness, and the bias power on the substrate. The detailed experimental conditions are listed in Table 2. Due to the low inductive power, the system worked in the capacitive mode (the so-called E-mode). A transition from MWCNTs to MWCNFs was observed when increasing the bias power on the lower substrate. Their global simulation showed an electron temperature and electron density of about 1.75 eV and ~10^{11} cm^{-3} at the conditions under study.
Cruden et al.[18] applied ultraviolet absorption and optical emission spectroscopy under conditions similar to[17] (see Table 2). The density of CH_3 detected in the plasma was in the order of 10^{13} cm^{-3}, and increased with pressure and power. The gas temperature was estimated between 700 and 1000K, i.e. less than the growth temperature of 1273 K on the substrate. An effective electron temperature of around 2.5-3.3eV was obtained.
Similar studies were performed by Matthews *et al.*[19] in the same ICP reactor as Delzeit but with a C_2H_4/H_2 mixture. Both MWCNTs and MWCNFs were synthesized. It was concluded that the bias power on the substrate played a key role in the transition from MWCNTs to MWCNFs. At a high substrate power free-standing MWCNFs could be grown. In addition, their results further indicated that the ion bombardment weakened the adhesion of the catalyst particles and lead to the tip growth mode under high substrate power.

An effort of synthesizing SWCNTs at low temperature in an ICP-PECVD system was reported by Yang and co-workers[20, 21]. The low ICP power was found more efficient for SWCNT growth under their conditions.

Ostrikov *et al*[22] used a low-frequency (0.46MHz) ICP-PECVD system to deposit carbon nanostructures with a mixture of $Ar/H_2/CH_4$. Their results indicated that the aligned carbon nanotip structures were predominantly grown by the molecular and radical units, whereas the plasma-grown nanoparticles were crucial components of polymorphous carbon films.
Vertically aligned carbon nanofibers were synthesized by Caughman *et al.*[23] using an ICP-PECVD system at 50 mTorr in a mixture of C_2H_2/H_2. The other conditions are listed in Table 2. They found that nanofibers grown in hydrogen-rich plasma tend to be straight and cylindrical, while those grown in carbon-rich plasma tend to be broad-based and conelike. Their optical emission measurements indicated that surface reactions play a key role in the plasma chemistry and that hydrogen and molecular carbon (C_2) could be related to the growth results.
Lin and co-workers reported an experimental investigation of an inductive C_2H_2/H_2 plasma under a pressure of 20 mTorr and 500 °C for CNF growth[24]. They have measured the intensities of C_2 species and H atoms by optical emission spectroscopy, as well as the energy and flux of ions incident on the substrate surface by an impedance meter. The line intensity of C_2 was found to increase with C_2H_2/H_2 ratio while the hydrogen atom density decreased accordingly. The relative density of C_2 and H atoms, as well as the ion current collected by the substrate electrode, increased with ICP power, which led to the increase of the growth rate of the CNFs. Moreover the etch effect upon the effective removing of the α-C on the catalyst surface is further enhanced by ion bombardment.
Wei[25] carried out a comprehensive study of the growth of vertically-aligned CNFs in an ICP-PECVD system under the conditions mentioned in Table 2. Mass spectroscopy was used to determine the plasma composition in the experiments. Long chain hydrocarbons were detected in their experiments, which poisoned the catalyst and prevented the growth of CNFs. The α-C on the catalyst surface could be efficiently removed by decreasing the gas pressure. The influence of dilution of NH_3 was also investigated.

To control CNT/CNF growth, it is necessary to have a good insight in the plasma behaviour. This can be obtained by computer simulations. Several efforts have been attempted in the past decades. A one-dimensional simulation was carried out by Hash *et al.*[26, 27] for a dc plasma used for CNT growth with a gas mixture of $Ar/C_2H_2/NH_3$. 24 species and 140 reactions were taken into account in their model. The simulation conditions were a pressure of 8 Torr, a flow rate of 100 sccm of argon, 50 sccm of NH_3 and 25 sccm of C_2H_2, $T_{substrate}$ of 700 °C, T_{wall} of 450 °C. A complete dissociation of NH_3 was observed in the simulations at relatively low bias of -325V. The Ar^+ ions were found the dominate ions followed by $C_2H_2^+$ and NH_4^+. The effect of bias on gas temperature was also discussed in the paper.
The amount of carbon in CNTs grown by a capacitvely coupled (CC) CH_4 plasma was predicted by Okita *et al.*[28] using one-dimensional fluid simulations combined with experimental measurements. The simulation results were consistent with experiment. The effects of hydrogen and pressure on the CNT formation in a CC CH_4/H_2 plasma was further investigated in [29]. H, CH_3, CH_5^+ and $C_2H_5^+$ were found to be the major radicals and ions, respectively. By analyzing the pressure dependence, the results suggested that both radical and non-radical neutrals played an important role as CNT growth precursors.
Denysenko *et al.*[30] performed detailed numerical simulations with a global model for depositing vertically aligned carbon nanostructures in an ICP-PECVD system. A gas mixture of $Ar/CH_4/H_2$ was used in their study. The densities and fluxes of radicals and charged species as well as the effective electron temperature, and methane conversion factor were calculated under various conditions. Their results showed that the deposited cation fluxes generally exceed those of the radical neutrals. The conversion rates of methane and hydrogen was found very high (~99%) in their study. Furthermore, Ostrikov *et al.*[31] reported a two-dimensional simulation of nanoassembly precursor species in an inductive $Ar/H_2/C_2H_2$ plasma. The number density and fluxes of the main building blocks and surface preparation species involved in the nanoassembly

of carbon-based nanopatterns were calculated in their study. They showed that the nanopattern quality might be affected by the process parameters and the non-uniformity of the surface fluxes of each particular species.
The current status of the technology of depositing CNTs by PECVD, including equipment, plasma chemistry, diagnostics and modelling, as well as mechanisms, was recently reviewed by Meyyappan[36]. It is stated that significant progress was achieved in the use of plasma-grown structures for various applications, but modelling efforts were very minimal[36].
From the literature review above, we can see that CNTs/CNFs could be synthesized under either moderate pressure (1~10 Torr) or low pressure (10s of mTorr) in a PECVD system (see Table 1 and 2). During the synthesis process, methane (CH_4) and acetylene (C_2H_2) are popular feedstock gases for the carbon source. A dilution by H_2 and NH_3 is often used to obtain hydrogen-rich plasmas, in order to produce 'clean' CNTs/CNFs. However, most of the above works focus on how to grow CNTs/CNFs in low-temperature PECVD, whereas the role of the plasma during the process of synthesizing CNTs/CNFs, as well as the key precursors for CNT growth, still remain more or less unclear.

To investigate the plasma chemistry for a CNT-PECVD system, a systematic study with the 2D Hybrid Plasma Equipment Model (HPEM)[37-42] is carried out in our group. An ICP reactor, more specifically, a transformer coupled plasma (TCP) reactor is used in the simulations for two reasons: first, the TCP system is widely used in the semiconductor industry, because it is simple to construct and offers high ionization efficiency compared to dc or RF capacitive discharges. In addition, the TCP reactor has an independent RF power supply to the substrate which can be useful in the growth of nanotubes in vertical alignment. Second, some experimental effort has been explored on synthesizing nanotubes in such system in the past decades[17-19]. These experimental data can be used to validate our simulation results.
Four kinds of feedstock gas mixtures (i. e., CH_4/H_2, CH_4/NH_3, C_2H_2/H_2, and C_2H_2/NH_3) are studied in this work for two different pressures: 50 mTorr and 1 Torr, corresponding to the low and moderate pressure range investigated in the experiments (see above and Table 2). The paper is organized as follows: a short description of the model is given in section 2, followed by the plasma chemistry of CH_4/H_2 (NH_3) and C_2H_2/H_2 (NH_3). In section 3, the numerical results are discussed. The conclusion and outlook will be summarized in section 4.

2. Description of the model

2.1. The Hybrid Plasma Equipment Model

The Hybrid Plasma Equipment Model (HPEM) has been developed at the University of Illinois by Kushner and coworkers[37-42] and addresses the plasma physics and chemistry in a modular fashion. The HPEM has been applied to a variety of reactor types in low temperature plasmas[43]. The main modules of HPEM are the Electromagnetic Module (EMM), Electron Energy Transport Module (EETM), and Fluid Kinetics Module (FKM). The plasma quantities are generated by iterating between these different coupled modules. A short review of these three modules is given in the following, more details can be found in the publications of Kushner *et al.*, the developers of the HPEM[37-42].
After defining the reactor geometry and initial operating conditions, the first module EMM calculates the electromagnetic fields within the reactor volume by solving Maxwell equations. These fields are used as inputs in the EETM, where the electron density, electron temperature, electron energy distribution function and electron impact reaction rates are computed with a Monte Carlo procedure or the Boltzmann equation. Subsequently, the FKM calculates densities and fluxes of the various plasma species (i.e. heavy particles and electrons) with continuity equations, and the electrostatic field with Poisson's equation. This electrostatic field is used as input again in the EMM. This cycle is iterated until convergence. The schematic of the modular HPEM is given in Fig. 1.

2.2 The plasma chemistry for CNT/CNF growth

As mentioned above, the plasma species densities are calculated with continuity equations, i.e., balance equation with different production and loss terms, determined by chemical reactions. The latter are specific for each gas mixture under study.

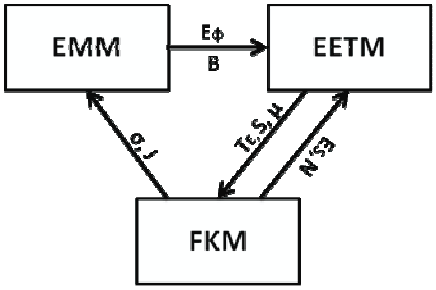

Figure 1. Schematic of the modular HPEM

a. Methane-hydrogen plasma chemistry (CH_4/H_2)
CH_4 and CH_4/H_2 plasmas have been used very frequently in ICP reactors for CNT formation in the past decades[15, 17, 18, 20, 21, 28-30].
After a sensitivity analysis, 33 species (electrons, ions, radicals and background neutrals) along with 58 electron impact reactions, 115 ion-neutral reactions, and 45 neutral-neutral reactions are taken into account in our model. The details are listed in Tables 3-6. Besides the inlet gas (CH_4/H_2), some higher order neutral molecules (C_3H_8, C_2H_6, C_2H_4, C_2H_2) are also included in our model, because they were found to be formed in the plasma at high densities[44]. Some radical and ionic species (e.g. C_3H_x, $C_3H_y^+$,…) as well as the negative ions are not incorporated in the model, although they might be present in a CH_4 plasma, but they have much lower densities. Note that the electron impact reactions are treated with energy dependent cross sections, whereas the ion and neutral reactions are described by rate coefficients.

b. Acetylene-hydrogen plasma chemistry (C_2H_2/H_2)
C_2H_2 is another popular gas used for the synthesis of carbon nano-films and carbon nanotubes[10-14, 23-27, 31]. Compared to methane, it can yield more highly polymerized ions and has a much stronger and faster tendency to form dust. The measurement of Deschenaux *et al.*[45] showed the formation of higher mass hydrocarbon cations and anions up to nearly 200 amu. The dominance of the species with an even carbon atom number is a distinct feature of C_2H_2 discharges.
One–dimensional fluid simulations of capacitive C_2H_2 plasmas have been performed for nanoparticle formation by De Bleecker *et al.*[46] and Mao *et al.*[47] in our group. The results showed that negative ions played a key role during the nanoparticle formation. However, the negative ions are not included in the current study because our preliminary simulations based on the mechanism proposed in [47] show that the magnitude of negative ions is at least one order smaller than that of electrons in an inductive acetylene discharge. Therefore the negative ions will not be considered in the current study to save computational effort.
Table 7 gives an overview of the 47 different species besides electrons considered in the model. The type of species included in the model is based on experimental observations of Deschenaux. *et al.*[45]. There are indeed more highly polymerized ions and neutrals included than in the CH_4/H_2 model (c.f. Table 3). 105 reactions involving 31 electron-impact reactions, 29 neutral-neutral reactions and 45 ion-neutral reactions are taken into account (see tables 8 -10).

c. Addition of ammonia (NH_3)
When NH_3 is used as dilution gas instead of H_2, an extra number of 22 species, 43 electron-impact reactions, 48 ion-neutral reactions and 67 neutral-neutral reactions were added to the model. All the details are given in tables 11-14.

2.3 Diffusion and wall deposition losses

Besides chemical reactions in the discharge, species can also be lost by diffusion to the reactor walls followed by deposition. The overall diffusion coefficient D_j of neutral species j in the gas mixture can be calculated by Blanc's law[48],

$$\frac{p_{tot}}{D_j} = \sum_i \frac{p_i}{D_{ij}} \tag{1}$$

where D_{ij} is the binary diffusion coefficient of species j in every background gas i [49],

$$D_{ij} = \frac{3}{16}\frac{k_B T_{gas}}{p_{tot}}\frac{4\pi k_B T_{gas}/m_{ij}^{1/2}}{\pi\sigma_{ij}^2 \Omega_D(\Psi)} \tag{2}$$

k_B is the Boltzmann constant, T_{gas} is the gas temperature in Kelvin, p_{tot} is the total gas pressure in Pascal, m_{ij} is the reduced molecular mass in amu, σ_{ij} is the binary collision diameter in Å.

$$\sigma_{ij} = \frac{\sigma_i + \sigma_j}{2} \tag{3}$$

and $\Omega_D(\Psi)$ is the diffusion collision integral given by[49]

$$\Omega_D = \frac{A}{\Psi^B} + \frac{C}{e^{D\Psi}} + \frac{E}{e^{F\Psi}} + \frac{G}{e^{H\Psi}} \tag{4}$$

with $\Psi = T_{gas}/\varepsilon_{ij}$, $\varepsilon_{ij} = (\varepsilon_i + \varepsilon_j)^{1/2}$ and constants A = 1.06036, B = 0.15610, C = 0.19300, D = 0.47635, E = 1.03587, F = 1.52996, G = 1.76464 and H = 3.89411. All data needed to calculate the diffusion coefficients of all the plasma species included in the models were adopted from [44] and [47].

For ions both motilities and diffusion coefficients are considered. The ion mobility of an ionic species j in the background gas i can be calculated from the low-electric-field Langevin mobility expression[48]

$$\mu_{ij} = 0.514 m_{ij}^{-0.5}\frac{T_{gas}}{P_{tot}}\alpha_i^{-0.5} \tag{5}$$

where α_i in $Å^3$ is the polarizability of the background gas and is taken from [44] and [47] for all ions. The overall ion mobility μ_j of ion j in the gas mixture can again be obtained by Blanc's law; see above. Finally, the ion diffusion coefficient can be derived from Einstein's relation

$$D_j^{\pm} = \frac{k_B T_{ion}}{e}\mu_j \tag{6}$$

where T_{ion} represents the ion temperature which is assumed to be equal to the gas temperature.

Finally, a sticking model, where the deposition of species at the wall is described, is applied to treat the plasma–wall interactions. The sticking coefficients assumed for the different radicals can be found in Table 15. For the ions a sticking coefficient of 1 is assumed, because they will be neutralized. For the molecules, a sticking coefficient of 0 is used, as they are considered to be reflected at the walls.

It should be noted that the same sticking model is also applied on the substrate. Indeed, due to the lack of reliable data, the same sticking coefficients are assumed on the substrate as on the other walls. This is of course an approximation, because the substrate for CNT growth is typically covered by metal catalyst nanoparticles (e.g., Ni, Fe, Al, Co; see Table 1 above), and it is generally assumed[50] that the hydrocarbon growth species will decompose at the surface of these nanoparticles. This represents a sink for the hydrocarbon species, which is included in the model by the sticking coefficients, but as the latter are taken as constant values, irrespective of the kind of wall material, it is an approximation.

The present work focuses mainly on the bulk plasma chemistry reactions. However, the model could be further improved by calculating detailed decomposition probabilities of the various hydrocarbon species at the nanoparticle surface, for instance by molecular dynamics simulations, and using these data as boundary conditions for the plasma chemistry model, in order to describe the process of CNT/CNF growth in more detail.

Alternatively, a separate model for the catalytic growth of CNTs, as was recently developed by Naha and Puri[51], could be combined to our plasma chemistry model. Such a model takes into account several mechanisms including adsorption and desorption of hydrocarbon species at the catalyst-gaseous hydrocarbon interface, surface and bulk diffusion, nucleation, and separation of solid undissolved carbon in nanostructured form. This model needs the predominant carbon-containing species density near the substrate as an input parameter, which is an output of our model. Vice versa, the surface processes provide the boundary conditions for the plasma chemistry model. In the near future, we would like to extend our plasma chemistry model, to take into account the decomposition of the hydrocarbon species at the catalyst nanoparticles in more detail.

3. Results and discussion

3.1. Operating conditions

The calculations were performed for eight cases, namely for four different gas mixtures: i.e., CH_4/H_2, CH_4/NH_3, C_2H_2/H_2, and C_2H_2/NH_3, and in each case for two different gas pressures: 50 mTorr representing the low-pressure range and 1 Torr for the moderate-pressure range. The gas ratio is always 20% for CH_4/C_2H_2 vs 80% H_2/NH_3. Other operating conditions are: 100 sccm total gas flow rate, 300 W source power, 30W bias power at the substrate electrode and an operating frequency of 13.56 MHz applied to the coil and to the substrate electrode. The substrate is heated to 550 °C. These are typical operating conditions for CNT growth, as was illustrated in Tables 1-2.

The reactor geometry under study is a TCP reactor, which is often used for CNT growth[17-19]. It is schematically illustrated in Figure 2.

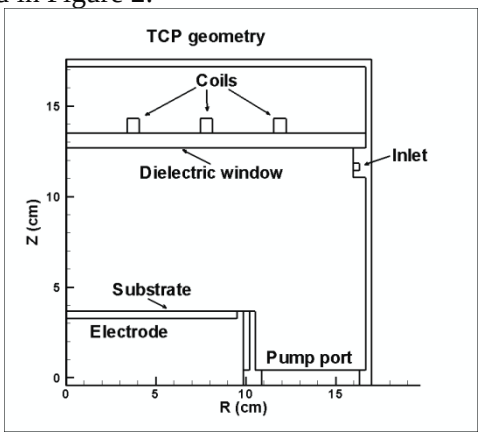

Figure 2: Two-dimensional TCP reactor geometry used in the model. The reactor is cylindrically symmetric, so only one half plane of the reactor is shown.

3.2. General calculation results

First we show some general calculated results, for the CH_4/H_2 gas mixture, at low pressure (50 mTorr) and moderate pressure (1 Torr). These results are representative for the other gas mixtures as well, unless mentioned otherwise.

The calculated 2D power density profiles at a pressure of 50 mTorr and 1 Torr are shown in figure 3 (a) and (b), respectively. The input power from the RF coil (i.e. 300W) is mainly deposited near the quartz windows below the coil. An off-axial peak is observed at both pressures. When the pressure is increased to 1 Torr, the region of power deposition becomes smaller compared to that at 50 mTorr. This reduction leads to higher peak values of power density at pressures of 1 Torr, because the total input power for both pressures is same (i.e. 300W). The peak values of power density are 0.36 and 0.55W/cm^3 at 50 mTorr and 1 Torr, respectively. In this region, the plasma electrons absorb the energy from the inductive electric field, which is called the “inductive region”.

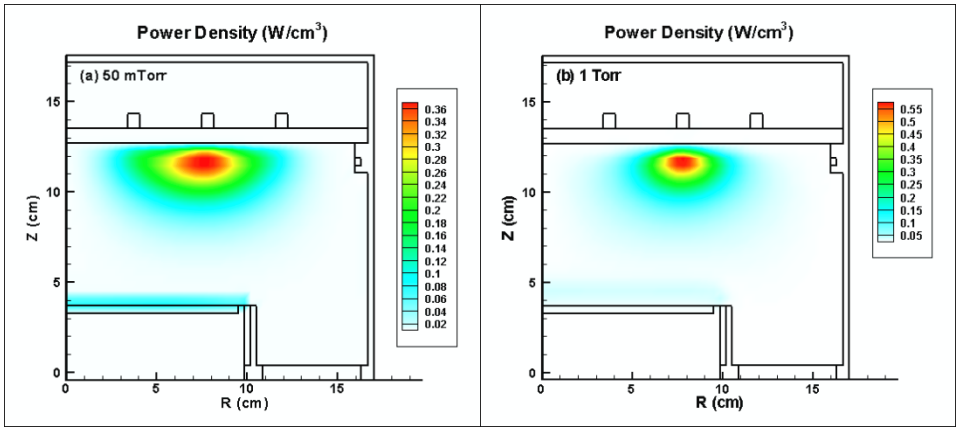

Figure 3 Calculated 2D power density profiles for a CH_4/ H_2 gas mixture at a pressure of (a) 50 mTorr and (b) 1 Torr with gas ratio of 20:80. The operation conditions are: 100 sccm gas flow rate, 300W source power, 30W bias power at the substrate and 13.56 MHz operating frequency at the coil and at the substrate electrode. The substrate is heated to 550 °C.

A second region of power deposition can be found above the substrate where the RF bias power of 30W is applied. It is clear from Fig. 3(a) and (b) that the power density in this region is fairly uniform. We call this region the "capacitive region" because the electrons absorb the energy mainly from the electrostatic field. The peak values of power density in this region are around 0.07 and 0.02 W/cm^3 at 50 mTorr and 1 Torr, respectively. Indeed at the moderate pressure of 1 Torr, the capacitive region is expanded, which results in a decrease of the maximum power density because the total power applied on the substrate is fixed as 30W for both pressures. Similar trends were also observed for the other three gas mixtures.

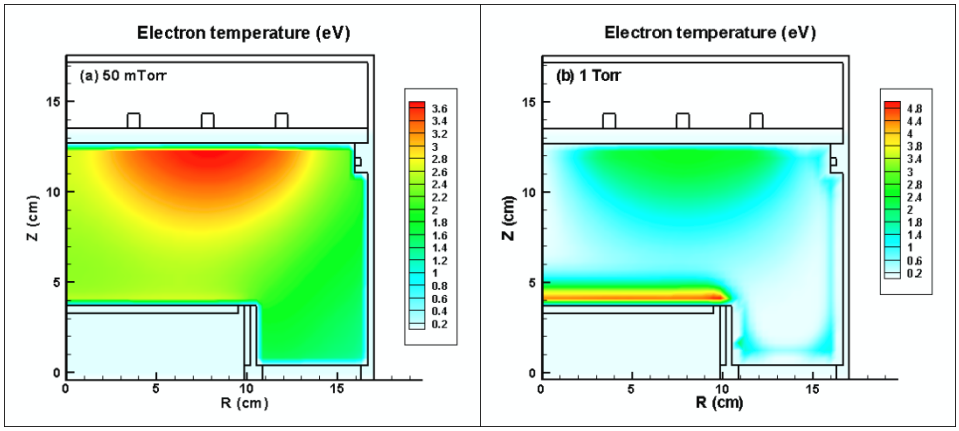

Figure 4 Calculated 2D electron temperature profiles at the same conditions as in figure 3

Figure 4 (a)-(b) displays the calculated 2D distributions of the electron temperature at the two different pressures. Similar to the power deposition, the electron temperature exhibits two peaks, i.e., in the inductive region and capacitive region, where the electrons gain energy from the electric field. At low pressure of 50 mTorr, the electron temperature shows values around 2.4~3.5 eV in the inductive region, which is comparable to the result measured by Cruden *et al.* in [18]. At the moderate pressure of 1 Torr, the values of electron temperature are reduced to 1~2.5 eV in the inductive region. These results are consistent with Delzeit *et al.*[17] and Ostrikov *et al.*[31]. In addition, the electron temperature remains as high as 4~6 eV in the capacitive region at 1 Torr. This can be explained because at higher pressure a lower electron density is found in the capacitive region (i.e., around 10 times lower than the density at 50 mTorr; see below). Hence, for a given applied bias power (30W), the electrons will be able to gain more energy.

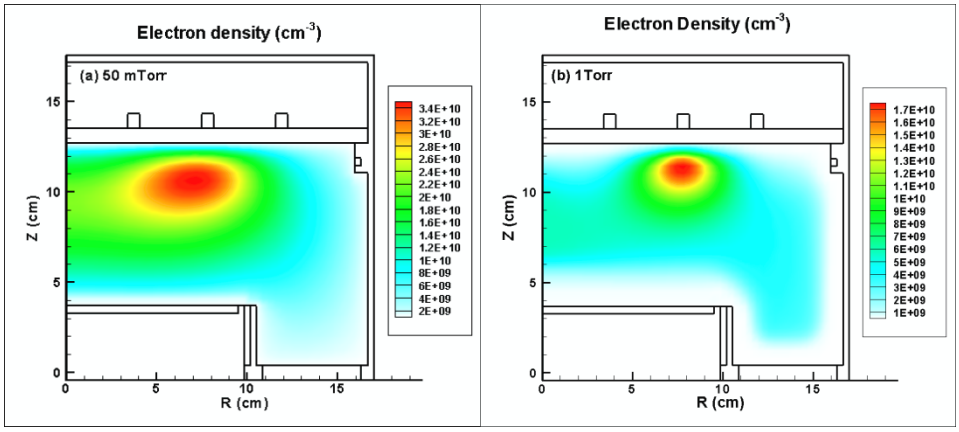

Figure 5 Calculated 2D electron density profiles at the same conditions as in figure 3

Figure 5 illustrates the calculated 2D profiles of the electron densities at the same conditions as in figure 3. Off-axial maxima are also observed for the electron density distribution. This is because in this region the electrons are created by the deposited power. When the pressure is increased to 1 Torr, the distribution of electrons becomes more localized. Indeed at high pressure, there are more collisions between electrons and the other species, so that the mean free path for electrons becomes smaller, and the electrons lose their energy much faster. At 50 mTorr, the electron density shows a peak value of 3.4×10^{10} cm^{-3} below the coil, and it decreases to 1×10^{9} cm^{-3} near the walls. Slightly higher values (i.e., 8.5×10^{10} cm^{-3} in a pure CH_4 ICP discharge at a pressure of 50 mTorr and a power of 500W) were reported by Bera *et al.*[52]. At the moderate pressure of 1 Torr, the peak value of electron density becomes 1.7×10^{10} cm^{-3}. This is because the large number of collisions between electrons and neutrals at the moderate pressure make electrons lose their energy much faster, leading to the reduction of high-energy electrons, which results in a decrease of the electron density.

The calculated 2D profiles of the gas temperature are plotted in figures 6(a)-(b). The substrate is heated to 823K (i.e. 550 °C). At the low pressure of 50 mTorr, the heat transfer towards the plasma is clearly displayed. The gas temperature gradually changes from 823 K at the substrate to about 600K in the bulk plasma, and reaches 324K at the wall. On the other hand, at the moderate pressure of 1Torr, the gas temperature sharply decreases near the substrate. Indeed, at higher pressure more “cooling” species are injected into the reactor (400K in our simulation), which leads to more species sharing the heat transferred from the substrate. Second, the collisions between the species become more frequent at higher pressure, so that the species lose their energy more quickly.

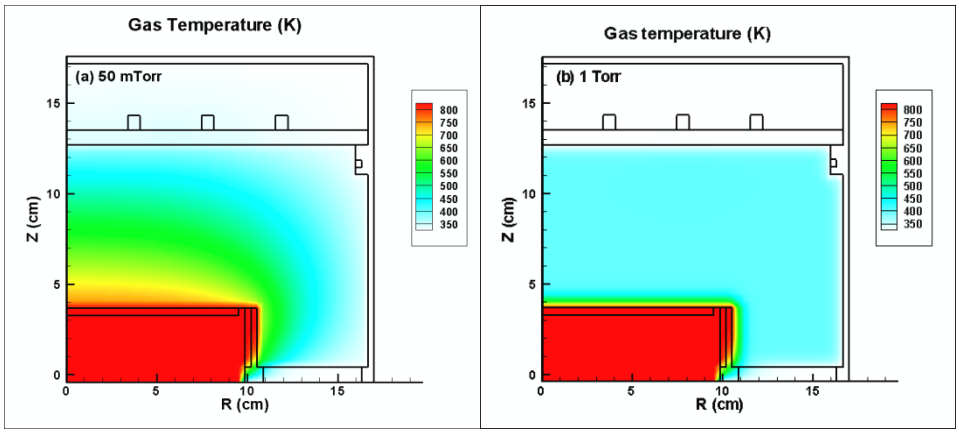

Figure 6 Calculated 2D gas temperature profiles at the same conditions as in figure 3.

The 2D number density distribution of the background gas CH_4 is displayed in figures 7 (a) and (b) at low and moderate pressure, respectively. The density reaches a maximum near the gas inlet and drops in the plasma due to ionization and dissociation reactions as shown in Table 4-6. The H-abstraction reaction $H + CH_4 \rightarrow H_2 + CH_3$ is found to be the predominant loss process. The rate constant for this reaction is very sensitive to the gas temperature (see Table 6) and its magnitude increases two orders when the gas temperature changes from 400 K to 900 K. Hence, this reaction is much faster at 50 mTorr where a higher gas temperature is reached (cf. figure 6 a and b). This explains why the CH_4 density does not drop so rapidly at 1 Torr, as is clear from fig. 7b.

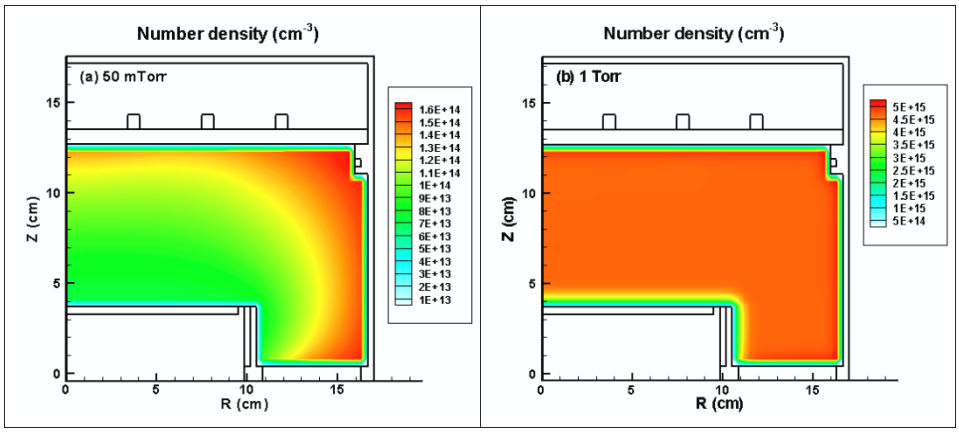

Figure 7 Calculated 2D number density of CH_4 at the same conditions as in figure 3.

Similar density profiles are also observed for the other background gases (i.e. C_2H_2, H_2 and NH_3; not shown in the paper). In the discharge, several new species are formed by ionization, dissociation and other reactions as given in table 3-14. These species will be discussed in the next section.

3.3. Plasma chemistry in the different gas mixtures

To analyze the role of the plasma chemistry for CNT/CNF growth in an ICP-PECVD system, the volume-averaged densities of all plasma components are calculated for the four different gas mixtures at the two pressures under study. The results are shown in figures 8-11 for the CH_4/H_2 plasma, the CH_4/NH_3 plasma, the C_2H_2/H_2 plasma, and the C_2H_2/NH_3 plasma, respectively.

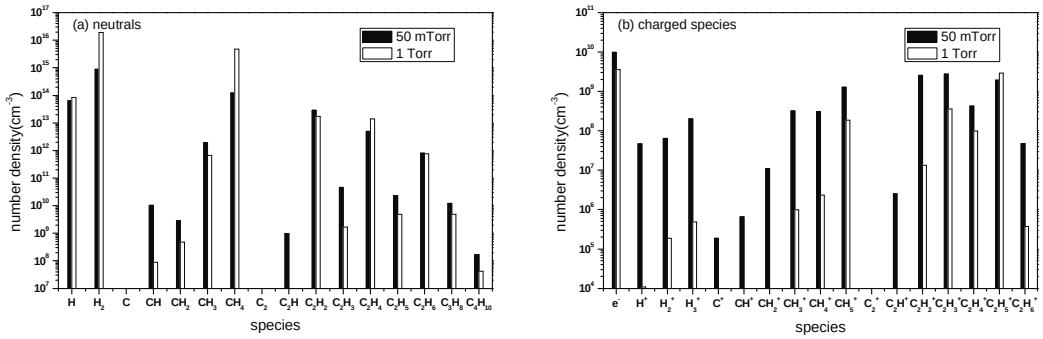

Figure 8. Calculated volume-averaged densities of (a) neutrals and (b) charged species for the CH_4/H_2 plasma at pressures of 50 mTorr and 1 Torr. The other parameters are the same as in figure 3.

In the CH_4/H_2 plasma, it is clear that H_2, C_2H_2 and C_2H_4 are the dominant molecules at both pressures, besides the feedstock gas CH_4. This is consistent with the results measured by Denysenko *et al.* using mass spectrometry in the pressue range of 20~70 mTorr[30]. The primary radicals are H and CH_3 at both pressures, which correlates well with the results of Oda et al.[29] At 50 mTorr, several ions are almost of equal importance, i.e., $C_2H_x^+$ (x=2,3,4,5) and

CH_x^+ (x=3,4,5), as well as H_3^+. In general, the ion densities are, however, five orders of magnitude lower than the neutrals densities, at 50 mTorr.
As the gas pressure increases to 1 Torr, the densities of H_2, CH_4 and C_2H_4 increase, but the density of C_2H_2 drops slightly. This is because the C_2H_2 molecules are mainly created by the following three reactions:

$$C_2H_4 + e^- \rightarrow C_2H_2 + H_2 + e^- \text{ (5.8 eV)}$$
$$CH + CH_2 \rightarrow H + C_2H_2$$
$$CH_2 + CH_2 \rightarrow H_2 + C_2H_2$$

Indeed, the densities of the radicals CH and CH_2, as well as the electrons densities decrease at higher pressures. The pressure effect is even more pronounced for all ions (except $C_2H_5^+$), which drop by one to three orders of magnitude. At the pressure of 1 Torr, $C_2H_5^+$ are the most important ions, followed by CH_5^+, $C_2H_3^+$ and $C_2H_4^+$. This behavior is correlated to the increase of the CH_4 and C_2H_4 densities. Indeed, these ions are mainly generated by reactions between small ions (such as H_2^+, H_3^+, CH_2^+ and CH_3^+) and the molecules CH_4 or C_2H_4 (see reactions 14, 18, 21, 22, 26, 28, 31, 34, 37 and 39 in Table 5). This also explains the significant drop in densities of H_2^+, H_3^+, $CH_2^+$and CH_3^+ ions.
It is known that CH_4 can hardly dissociate on the catalyst surface, whereas C_2H_2, C_2H_4 and C_2H_6 are characterized by a lower decomposition temperature[50]. Hence, because these molecules are also present in high densities in the CH_4/H_2 plasma, they will probably serve as carbon source for CNT/CNF growth. Moreover, as the hydrocarbon radicals are thought to be typical growth precursors for amorphous carbon thin films[52], a significant drop in their densities when increasing the pressure might indicate that a "cleaner" environment for CNT/CNF growth could be obtained. This might explain why a higher growth rate of CNT/CNF could be achieved at higher pressure[12].

When NH_3 is diluted into the CH_4 plasma instead of H_2, the hydrocarbon species, such as C_mH_n ($0 \le m \le 3$, $0 \le n \le 8$) and $C_xH_y^+$ show similar trends as in the CH_4/H_2 plasma, i.e., the densities of the molecules H_2, CH_4, C_2H_4 and C_2H_6 increase with pressure, whereas the densities of most hydrocarbon radicals and ions show a decreasing trend. It is apparent that the densities of H_2 and H reach the same value as in the case when hydrogen was used as the dilution gas. Indeed, these H_2 molecules arise now mainly from the NH_3 feedstock gas, by H abstraction reactions (see reaction 2 and 3 in Table 14) and the three body recombination reaction ($H + H + NH_3 \rightarrow H_2 + NH_3$). As will be shown later, the ammonia is indeed highly decomposed in the plasma.

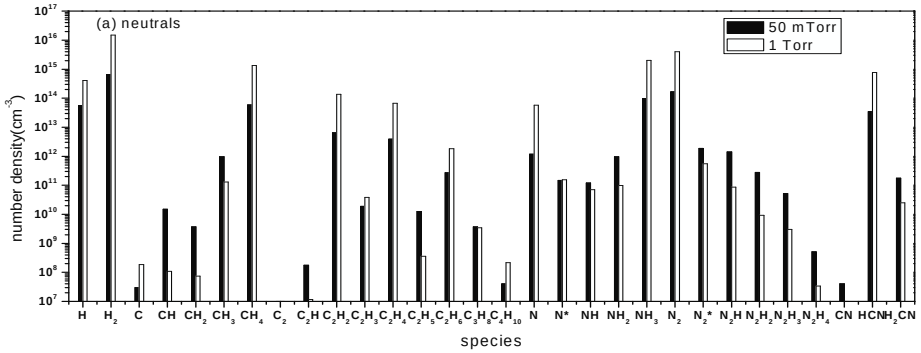

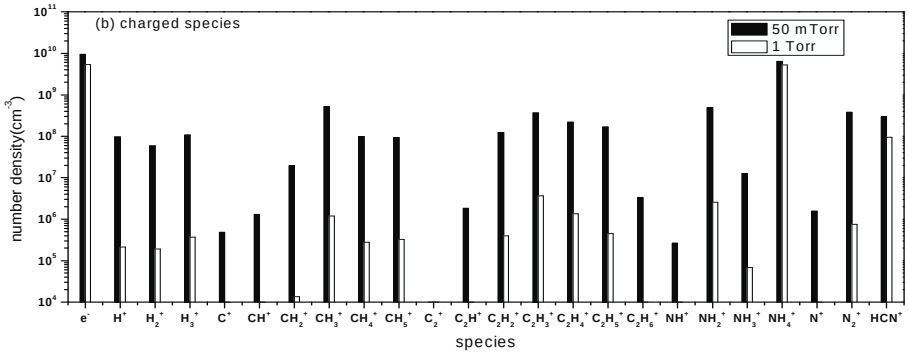

Figure 9 Calculated volume-averaged densities of (a) neutrals and (b) charged species for the CH_4/NH_3 plasma at pressures of 50 mTorr and 1 Torr. The other parameters are the same as in figure 3.

Moreover, the neutral species of N_2 and HCN, besides the NH_3 feedstock gas, are observed at relatively high densities. This is consistent with the results reported by Bell *et al.* [13]. Indeed, H_2, N_2 and HCN were detected as major neutral species when CNTs were synthesized in the C_2H_2/NH_3 plasma. The role of NH_3 was also discussed in that paper: it was stated to be a more effective source of atomic hydrogen compared with H_2. Also from our calculations it is clear that H atoms are formed to a large extent when NH_3 is used as the dilution gas (see figure 9a). In addition, a significant amount of atomic nitrogen is also predicted by our model, and this activated nitrogen can also affect the growth kinetics of CNT/CNF at the catalyst surface[53]. Finally, the NH_4^+ ions are found to be the dominant ions, which agree well with the simulation results of Hash et al. [26, 27].

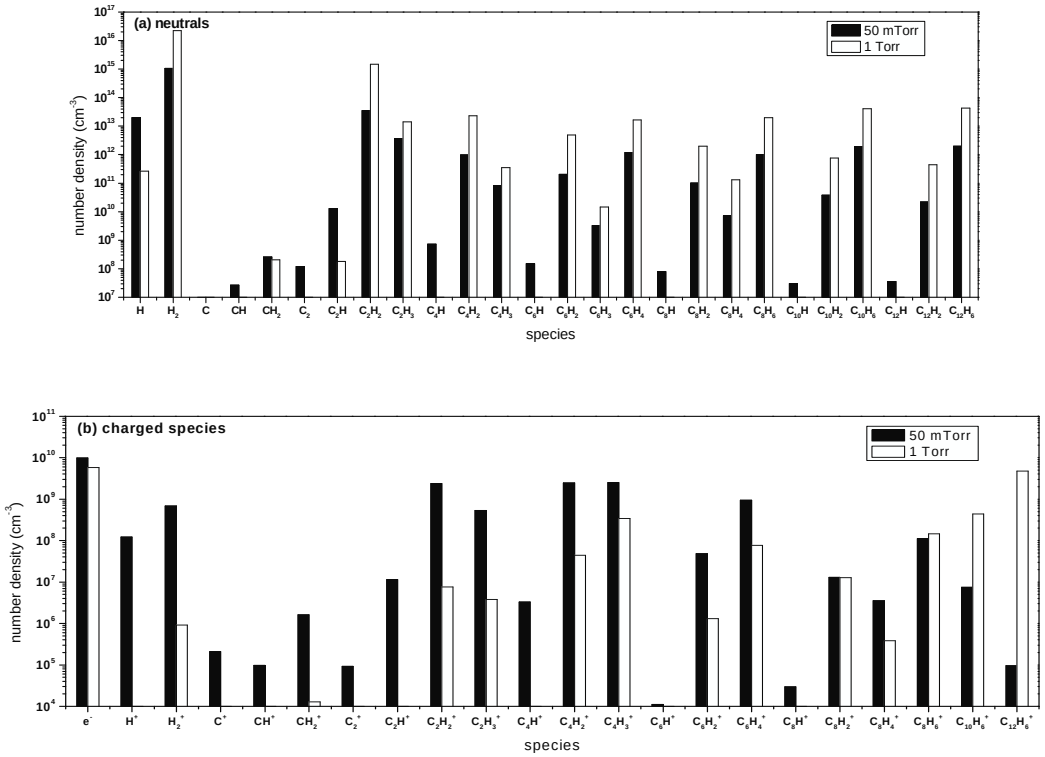

Figure 10 Calculated volume-averaged densities of (a) neutrals and (b) charged species for the C_2H_2/H_2 plasma at pressures of 50 mTorr and 1 Torr. The other parameters are the same as in figure 3.

In the acetylene/hydrogen plasma (see figure 10), long-chain hydrocarbons such as $C_{2n}H_2$ and $C_{2n}H_6$ (n=4,…,6) are formed in the discharge, and become important for both pressures. This has been reported also by Wei [25] using mass spectrometry, and it was stated that they poisoned the catalyst and prevented the growth of CNFs[25] The major ions are $C_2H_2^+$, $C_4H_2^+$, $C_4H_3^+$, and

$C_6H_4^+$ at low pressure. At the pressure of 1 Torr, the $C_{2n}H_6^+$ (n =4,…,6) ions become predominant. Indeed, these heavy ions are primarily created from C_2H_2 insertion reactions (see 24-27 in Table 9). These heavy ions will probably enhance the physical sputtering on the surface of the catalyst to remove the amorphous C film. In addition, these energetic ions may weaken the adhesion of catalyst particles, leading to the tip growth mode during the CNF formation[50].

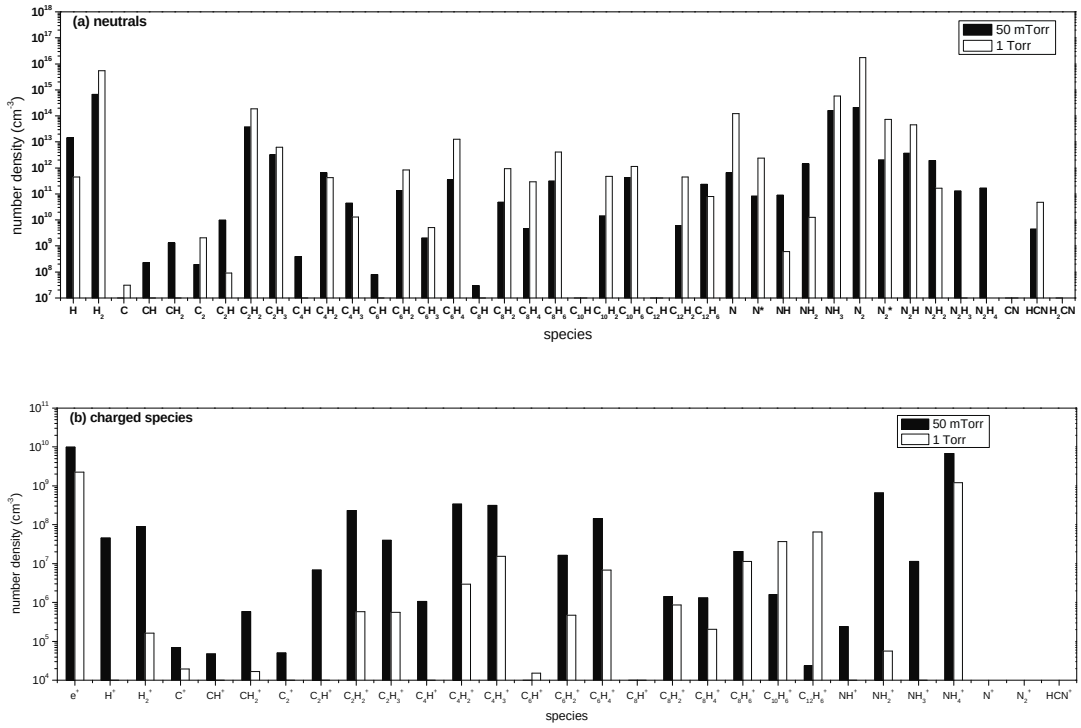

Figure 11 Calculated volume-averaged densities of (a) neutrals and (b) charged species for the C_2H_2/NH_3 plasma at pressures of 50 mTorr and 1 Torr. The other parameters are the same as in figure 3.

In the C_2H_2/NH_3 discharge, on the other hand, the formation of long chain hydrocarbons is less important, as is clear from figure 11. N_2 and NH_4^+ are the predominant neutrals and ions, respectively. Compared with the CH_4/NH_3 plasma, the densities of H and H_2 are reduced with one order of magnitude, and more striking is the drop in H density upon pressure increase, which is opposite to the behavior in the CH_4/NH_3 plasma (see above). The atomic hydrogen is commonly accepted as an etchant during the CNT/CNF growth. The decrease in density of H would reduce the etching effect in CNT/CNF growth, resulting in the enhanced CNT/CNF growth[54].

In general, we can see that atomic carbon is hardly formed in the plasma, for the four gas mixtures under study at two different gas pressures. Therefore we can conclude that the carbon sources for CNT/CNF growth mainly arise from decomposition of hydrocarbon molecules on the catalyst surface, as is also stated in [55].

To examine the conversion of the background gases, the decomposition rate (DR) is defined as follows

$$DR=1-\frac{\text{volume-averaged density of background gas}}{\text{density of background gas at inlet}} \quad (7)$$

The calculated results for the four different gas mixtures at the two different pressures are shown in Table 16.

It is clear from the table that the background CH_4/C_2H_2 gases have a higher DR (more than 71%) when ammonia is used as the dilution gas. Moreover, the ammonia itself also almost fully converted (more than 83%), which was also observed in [26]. Compared to the ammonia

dilution, the hydrogen has almost no decomposition (around 0.2~9% in the case of CH_4 and even negative values in the case of C_2H_2). These negative values mean that more background gas species are formed than decomposed. Indeed, the threshold energy needed for the dissociation of CH_4/C_2H_2 (8.8/7.5 eV) is slightly lower than that for H_2 (8.87eV). Hence, H_2 can be formed due to dissociation of CH_4/C_2H_2, followed by recombination of the resulting H atoms into H_2.
As far as the pressure effects are concerned, the background gas CH_4 has more or less the same DR in case of ammonia dilution, and C_2H_2 has a slightly higher DR at the pressure of 1 Torr compared to 50 mTorr when ammonia is used as the dilution gas. However when hydrogen is the dilution gas, a significantly lower DR of the background gases was observed at the higher pressure. This is most striking for the CH_4/H_2 plasma, where the DR of CH_4 drops from almost 50% at 50 mTorr to 3% at 1 Torr. Because CH_4 can hardly dissociate on the catalyst surface [50], this would suggest that the carbon source for CNT growth is very small in the CH_4/H_2 plasma at the moderate pressure range of around 1 Torr. This might be correlated with literature [20, 21] where such conditions were found to be favourable for the formation of SWCNT.

4. Conclusions

An ICP reactor operating in four different gas mixtures and at two pressures in the range typically used for CNT/CNF growth was investigated by means of hybrid plasma simulations. The feedstock hydrocarbon source gases were decomposed in the plasma, generating small and reactive ions and neutrals. The latter can reach the substrate to provide the carbon sources for CNT/CNF growth.
It was found that in methane containing plasmas the radicals H and CH_3 are the primary radicals, C_2H_2 and C_2H_4 (and N_2 and HCN in case of ammonia dilution) are the dominant molecules besides the feedstock gases (H_2/NH_3 and CH_4). Several ions, i.e., CH_x^+ (x=3, 4, 5) and $C_2H_x^+$ (x=2, 3, 4, 5), are of comparable importance. The densities of the molecules increase with pressure, while the radical and ion densities become lower at higher pressures. Our results suggest that C_2H_2 and C_2H_4 are the main precursors for CNT/CNF growth in methane containing plasmas.
On the other hand in acetylene containing plasma, the long chain species (both neutrals and ions) are predominant. The latter will enhance the physical sputtering and it can therefore be expected that they can effectively remove amorphous C films on the catalyst particles. Therefore, these long chain species probably play a key role in the formation of CNTs/CNFs.
When ammonia was used as the dilution gas, the trends of hydrocarbon species were found similar as in the H_2-dilution plasmas, but the N_2 and NH_4^+ species became the dominant neutrals and ions, respectively. A significant amount of atomic nitrogen was also predicted in our model, and these reactive nitrogen species can also affect the growth kinetics of CNTs/CNFs at the catalyst surface.
Our simulations suggest that, under the investigated operating conditions, a high DR of the hydrocarbon feedstock gases (either CH_4 or C_2H_2) can be achieved when NH_3 is used as the dilution gas, for both low and moderate pressure, as well as in the case of H_2 dilution at low pressure. However, at the moderate pressure of 1 Torr, the DR of CH_4 is very low in the case of H_2 dilution. Because CH_4 cannot easily be dissociated at the catalyst surface, this suggests that the carbon source for CNT formation is rather limited, which could correspond to conditions favorable for SWCNT growth, as is indeed observed in literature [20, 21].
In all cases investigated, the density of atomic carbon in the plasma is found to be very low; hence the C-supply for the CNT/CNF growth needs to come from decomposition of hydrocarbon species at the catalyst surface itself, as is also generally stated in literature[55]. The detailed behavior of the hydrocarbon species at the catalyst surface is not yet taken into account in our model. Indeed, our model only provides insight in the most important plasma species present in the discharge, which might play a role for the CNT growth. However, in future work, we would like to combine our plasma chemistry model, providing the fluxes of the most important plasma species to the substrate, with a model describing the surface processes on the catalyst nanoparticles, in order to obtain a comprehensive picture of the catalytic growth of CNTs.

5. Acknowledgements

We would like to thank the Fund for Scientific Research (FWO Flanders) and the Prime Minister's Office through IUAP-VI for financial support as well as the CalcUA computing facilities of the University of Antwerp. We are also very grateful to M. Kushner and group members for providing the HPEM and useful advice.

References

[1] Iijima S 1991 *Nature* **354** 56-8.
[2] Tseng G Y and Ellenbogen J C 2001 *Science* **294** 1293-4.
[3] Darkrim F L, Malbrunot P and Tartaglia G P 2002 *International Journal of Hydrogen Energy* **27** 193-202.
[4] Guillorn M A, Melechko A V, Merkulov V I, Ellis E D, Simpson M L, Baylor L R and Bordonaro G J 2001 *Journal of Vacuum Science & Technology B* **19** 2598-601.
[5] Meyyappan M, Delzeit L, Cassell A and Hash D 2003 *Plasma Sources Science & Technology* **12** 205-16.
[6] Journet C, Maser W K, Bernier P, Loiseau A, delaChapelle M L, Lefrant S, Deniard P, Lee R and Fischer J E 1997 *Nature* **388** 756-8.
[7] Yudasaka M, Komatsu T, Ichihashi T and Iijima S 1997 *Chemical Physics Letters* **278** 102-6.
[8] Lee C J, Kim D W, Lee T J, Choi Y C, Park Y S, Lee Y H, Choi W B, Lee N S, Park G S and Kim J M 1999 *Chemical Physics Letters* **312** 461-8.
[9] Cui H, Zhou O and Stoner B R 2000 *J Appl Phys* **88** 6072-4.
[10] Bower C, Zhu W, Jin S H and Zhou O 2000 *Appl Phys Lett* **77** 830-2.
[11] Gulas M, Le Normand F and Veis P 2009 *Applied Surface Science* **255** 5177-80.
[12] Chhowalla M, Teo K B K, Ducati C, Rupesinghe N L, Amaratunga G A J, Ferrari A C, Roy D, Robertson J and Milne W I 2001 *J Appl Phys* **90** 5308-17.
[13] Bell M S, Lacerda R G, Teo K B K, Rupesinghe N L, Amaratunga G A J, Milne W I and Chhowalla M 2004 *Appl Phys Lett* **85** 1137-9.
[14] Hofmann S, Ducati C, Robertson J and Kleinsorge B 2003 *Applied Physics Letters* **83** 135-7.
[15] Okita A, Suda Y, Oda A, Nakamura J, Ozeki A, Bhattacharyya K, Sugawara H and Sakai Y 2007 *Carbon* **45** 1518-26.
[16] Hiramatsu M, Shiji K, Amano H and Hori M 2004 *Applied Physics Letters* **84** 4708-10.
[17] Delzeit L, McAninch I, Cruden B A, Hash D, Chen B, Han J and Meyyappan M 2002 *J Appl Phys* **91** 6027-33.
[18] Cruden B A and Meyyappan M 2005 *J Appl Phys* **97** 084311--15.
[19] Matthews K, Cruden B A, Chen B, Meyyappan M and Delzeit L 2002 *J Nanosci Nanotechno* **2** 475-80.
[20] Weng C H, Yang C S, Lin H, Tsai C H and Leou K C 2008 *Journal of Nanoscience and Nanotechnology* **8** 2526-33.
[21] Yang C S 2005 Low temperature growth of single-walled carbon nanotubes by PECVD. In: *Department of Engineering and System Science,* (Hsinchu, Taiwan: National Tsing Hua University) p 88.
[22] Ostrikov K, Tsakadze Z, Rutkevych P P, Long J D, Xu S and Denysenko I 2005 *Contributions to Plasma Physics* **45** 514-21.
[23] Caughman J B O, Baylor L R, Guillorn M A, Merkulov V I, Lowndes D H and Allard L F 2003 *Appl Phys Lett* **83** 1207-9.
[24] Lin Y Y, Wei H W, Leou K C, Lin H, Tung C H, Wei M T, Lin C and Tsai C H 2006 *J Vac Sci Technol B* **24** 97-103.
[25] Wei H W 2008 study of growth of vertically-aligned carbon nanofibers by plasma enhanced chemical vapor deposition growth mechanism and field emission characterization. In: *Department of Engineering and System Science,* (Hsinchu, Taiwan: National Tsing Hua University) p 175.
[26] Hash D, Bose D, Govindan T R and Meyyappan M 2003 *J Appl Phys* **93** 6284-90.
[27] Hash D B, Bell M S, Teo K B K, Cruden B A, Milne W I and Meyyappan M 2005 *Nanotechnology* **16** 925-30.
[28] Okita A, Suda Y, Ozeki A, Sugawara H, Sakai Y, Oda A and Nakamura J 2006 *J Appl Phys* **99** 0143021-7.
[29] Oda A, Suda Y and Okita A 2008 *Thin Solid Films* **516** 6570-4.
[30] Denysenko I B, Xu S, Long J D, Rutkevych P P, Azarenkov N A and Ostrikov K 2004 *J Appl Phys* **95** 2713-24.
[31] Ostrikov K, Yoon H J, Rider A E and Vladimirov S V 2007 *Plasma Process Polym* **4** 27-40.
[32] Teo K B K, Lacerda R G, Yang M H, Teh A S, Robinson L A W, Dalal S H, Rupesinghe N L, Chhowalla M, Lee S B, Jefferson D A, Hasko D G, Amaratunga G A J, Milne W L, Legagneux P, Gangloff L, Minoux E, Schnell J P and Pribat D 2004 *Iee Proceedings-Circuits Devices and Systems* **151** 443-51.
[33] Koohsorkhi J, Hoseinzadegan H, Mohajerzadeh S, Soleimani E A, Koohsorkhi J and Arzi E 2005 *Fullerenes Nanotubes and Carbon Nanostructures* **13** 355-64.

[34] Shimoi N and Tanaka S 2008 *Journal of Ceramic Processing Research* **9** 437-9.
[35] Cassell A M, Ye Q, Cruden B A, Li J, Sarrazin P C, Ng H T, Han J and Meyyappan M 2004 *Nanotechnology* **15** 9-15.
[36] Meyyappan M 2009 *J Phys D Appl Phys* **42** 213001-15.
[37] Ventzek P L G, Sommerer T J, Hoekstra R J and Kushner M J 1993 *Appl Phys Lett* **63** 605-7.
[38] Collison W Z and Kushner M J 1996 *Appl Phys Lett* **68** 903-5.
[39] Kushner M J, Collison W Z, Grapperhaus M J, Holland J P and Barnes M S 1996 *J Appl Phys* **80** 1337-44.
[40] Grapperhaus M J and Kushner M J 1997 *J Appl Phys* **81** 569-77.
[41] Rauf S and Kushner M J 1997 *J Appl Phys* **81** 5966-74.
[42] Kinder R L and Kushner M J 2001 *J Vac Sci Technol A* **19** 76-86.
[43] Kushner M J 2009 *J Phys D Appl Phys* **42** 194013--20.
[44] Herrebout D, Bogaerts A, Yan M, Gijbels R, Goedheer W and Vanhulsel A 2002 *J Appl Phys* **92** 2290-5.
[45] Deschenaux C, Affolter A, Magni D, Hollenstein C and Fayet P 1999 *J Phys D Appl Phys* **32** 1876-86.
[46] De Bleecker K, Bogaerts A and Goedheer W 2006 *Physical Review E* **73** 026405--16.
[47] Mao M, Benedikt J, Consoli A and Bogaerts A 2008 *J Phys D Appl Phys* **41** 225201--14.
[48] Thomson G M, Schummer.Jh, James D R, Graham E, Gatland I R, Flannery M R and Mcdaniel E W 1973 *J Chem Phys* **58** 2402-11.
[49] Ervin K M, Ho J and Lineberger W C 1989 *J Chem Phys* **91** 5974-92.
[50] Hash D B and Meyyappan M 2003 *J Appl Phys* **93** 750-2.
[51] Naha S and Puri I K 2008 *J Phys D Appl Phys* **41** -.
[52] Bera K, Farouk B and Vitello P 2001 *J Phys D Appl Phys* **34** 1479-90.
[53] Jung M J, Eun K Y, Baik Y J, Lee K R, Shin J K and Kim S T 2001 *Thin Solid Films* **398** 150-5.
[54] Lee T Y, Han J H, Choi S H, Yoo J B, Park C Y, Jung T, Yu S, Yi W K, Han I T and Kim J M 2003 *Diam Relat Mater* **12** 851-5.
[55] Hofmann S, Sharma R, Ducati C, Du G, Mattevi C, Cepek C, Cantoro M, Pisana S, Parvez A, Cervantes-Sodi F, Ferrari A C, Dunin-Borkowski R, Lizzit S, Petaccia L, Goldoni A and Robertson J 2007 *Nano Lett* **7** 602-8.
[56] Hayashi M 1979 *J Phys-Paris* **40** 45-6.
[57] Kline L E 1982 *Ieee T Plasma Sci* **10** 224-33.
[58] Sohn W, Kochen K H, Scheuerlein K M, Jung K and Ehrhardt H 1986 *Journal of Physics B: Atomic and Molecular Optical Physics* **19** 3625-32.
[59] Tanaka H, Kubo M, Onodera N and Suzuki A 1983 *J Phys B-at Mol Opt* **16** 2861-9.
[60] Winters H F 1975 *J Chem Phys* **63** 3462-6.
[61] Chatham H, Hils D, Robertson R and Gallagher A 1984 *The Journal of Chemical Physics* **81** 1770-7.
[62] Reiter R K J a D 2002 *FZJ Report* **Juel-3966**
[63] Reiter R K J a D 2002 *FZJ Report* **Juel-4005**
[64] Tawara H, Itikawa Y, Nishimura H, Tanaka H and Nakamura Y 1992 *Nucl Fusion* **2** 41-64.
[65] Tian C C and Vidal C R 1998 *J Phys B-at Mol Opt* **31** 895-909.
[66] UMIST *http://www.udfa.net/*
[67] Herrebout D, Bogaerts A, Yan M, Gijbels R, Goedheer W and Dekempeneer E 2001 *J Appl Phys* **90** 570-9.
[68] Morrison N A, William C and Milne W I 2003 *J Appl Phys* **94** 7031-43.
[69] http://physics.nist.gov/PhysRefData/Ionization/molTable.html.
[70] Laufer A H and Fahr A 2004 *Chem Rev* **104** 2813-32.
[71] Wang H and Frenklach M 1997 *Combust Flame* **110** 173-221.
[72] Masi M, Cavallotti C and Carra S 1998 *Chem Eng Sci* **53** 3875-86.
[73] Frenklach M and Warnatz J 1987 *Combust Sci Technol* **51** 265-83.
[74] Landera A, Krishtal S P, Kislov V V, Mebel A M and Kaiser R I 2008 *J Chem Phys* **128** -.
[75] Hayashi M 1990 *Nato Adv Sci I B-Phy* **220** 333-40.
[76] Hack W and Wagner H G 1994 *Ber Bunsen Phys Chem* **98** 156-64.
[77] Thielen K and Roth P 1986 *Aiaa J* **24** 1102-5.
[78] Corchado J C and EspinosaGarcia J 1997 *J Chem Phys* **106** 4013-21.
[79] Sommerer T J and Kushner M J 1992 *J Appl Phys* **71** 1654-73.
[80] Rohrig M and Wagner H G 1994 *Ber Bunsen Phys Chem* **98** 858-63.
[81] Kushner M J 1992 *J Appl Phys* **71** 4173-89.

[82] Stothard N, Humpfer R and Grotheer H H 1995 *Chem Phys Lett* **240** 474-80.
[83] Xu Z F, Fang D C and Fu X Y 1998 *Int J Quantum Chem* **70** 321-9.
[84] Pagsberg P B, Eriksen J and Christensen H C 1979 *J Phys Chem-Us* **83** 582-90.
[85] Meaburn G M and Gordon S 1968 *J Phys Chem-Us* **72** 1592-&.
[86] Nicholas J E, Spiers A I and Martin N A 1986 *Plasma Chem Plasma P* **6** 39-51.
[87] Xu Z F, Fang D C and Fu X Y 1997 *Chem Phys Lett* **275** 386-91.
[88] Yoshimura M, Tamura F, Koshi M and Matsui H 1990 *Nippon Kagaku Kaishi* 589-93.
[89] Teng L and Winkler C A 1973 *Can J Chem* **51** 3771-3.
[90] Linder D P, Duan X F and Page M 1996 *J Chem Phys* **104** 6298-307.
[91] Gehring M, Hoyerman.K, Wagner H G and Wolfrum J 1971 *Berich Bunsen Gesell* **75** 1287-&.
[92] Schiavello M and Volpi G G 1962 *J Chem Phys* **37** 1510-&.
[93] Stief L J 1970 *J Chem Phys* **52** 4841-&.
[94] Vaghjiani G L 1995 *Int J Chem Kinet* **27** 777-90.
[95] Dorai R and Kushner M J 2003 *J Phys D Appl Phys* **36** 666-85.
[96] Legrand J C, Diamy A M, Hrach R and Hrachova V 1998 *Vacuum* **50** 491-5.
[97] Legrand J C, Diamy A M, Hrach R and Hrachova V 1997 *Vacuum* **48** 671-5.
[98] Okita A, Suda Y, Ozeki A, Sugawara H, Sakai Y, Oda A and Nakamura J 2006 *J Appl Phys* **99** -.
[99] Naujoks D, Bohmeyer W, Markin A, Arkhipov I, Carl P, Koch B, Reiner H D, Schroder D and Fussmann G 2004 *Phys Scripta* **T111** 80-5.
[100] Liu D P, Martin I T, Zhou J and Fisher E R 2006 *Pure Appl Chem* **78** 1187-202.

Table 1. Overview of different plasma sources used for the synthesis of CNTs/CNFs by PECVD

No.	Plasma source	Gas mixture	Pressure	Substrate temperature	Bias power	Catalyst	Carbon structure	Reference
Experiments:								
1	MW	CH_4/NH_3	21 Torr	650~1000 °C	no	Fe	MWCNTs	[9]
2	MW	C_2H_2/NH_3	20 Torr	825 °C	no	Fe (or Co, Ni)/γ-Al_2O_3	MWCNTs	[10]
3	HF	C_2H_2/ NH_3/ H_2	7.5 Torr	700 °C	no	Fe	MWCNTs	[11]
4	dc	C_2H_2/NH_3	3.5 Torr	700 °C	yes	Ni/Co	MWCNTs	[12]
5	dc	C_2H_2/NH_3	1.875 Torr	650 °C	yes	Ni	MWCNTs	[13]
6	dc	C_2H_2/NH_3	1.125 Torr	270 °C/500 °C	yes	Ni	MWCNFs	[14]
7	CCP	CH_4/H_2	1~10 Torr	650 °C	yes	Al_2O_3/Fe/Al_2O_3	MWCNTs	[15]
8	CCP	C_2F_6/H_2	100 mTorr	500 □C	yes	Ni	Carbon Nanowalls	[16]
9	ICP	CH_4/H_2	0.5~20 Torr	800 ~1000 °C	yes	Al/Fe	MWCNTs/MWCNFs	[17]
10	ICP	C_2H_4/H_2	3 Torr	900 °C	yes	Al/Fe	MWCNTs/MWCNFs	[18, 19]
11	ICP	CH_4/H_2	1 Torr	500 ~650 °C	no	Fe/Al, Ni/Al	SWCNT	[20, 21]
12	ICP	CH_4/H_2/Ar	30~50 mTorr	300 ~500 °C	yes	Ni	Carbon nanostructures	[22]
13	ICP	C_2H_2/H_2	50 mTorr	700 °C	yes	Ni	MWCNFs	[23]
14	ICP	C_2H_2/H_2	20 mTorr	500 °C	yes	Ni	MWCNFs	[24]
15	ICP	C_2H_2/H_2	17 mTorr	550~650 °C	no	Ni	MWCNFs	[25]
Modelling:								
16	dc	Ar /C_2H_2/NH_3	8 Torr	700 °C	yes	-	CNTs	[26, 27]
17	CCP	CH_4/H_2	1~10 Torr	650 °C	yes	-	CNTs	[28, 29]
18	ICP	Ar/CH_4/ H_2	<100 mTorr	300 °C	no	-	Carbon nanostructures	[30]
19	ICP	Ar /C_2H_2/H_2	100 mTorr 1~7 Torr	27 °C	no	-	Carbon nanostructures	[31]

Table 2. Detailed overview of the progress achieved in ICP-PECVD for CNT/CNF growth. The numbers given in the first column correspond to the numbers in the first column of Table 1.

No.	ICP-Power frequency	Pressure	Gas mixture (gas ratio)	Flow rate	Bias-power frequency	Substrate temperature	Study methods	Plasma properties	Some conclusions	Reference
9	0~200 W 13.56 MHz	0.5~20 Torr	CH_4/H_2 (20/80)	100 sccm	0~120 W 13.56 MHz	800 °C	OES and 0D Global modelling	n_e~10^{11} cm^{-3} T_e~1.75 eV	A transition occurs from CNTs to CNFs by varying bias-power	[17]
9	0~200W 13.56MHz	0.5~20 Torr	CH_4/H_2 (20/80)	100 sccm	0~110W 13.56MHz	1000 °C	OES, UV absorption spectroscopy	T_{gas}=700 ~1100 K n_{CH3}~10^{13} cm^{-3} T_e=2.5~3.3 eV		[18]
10	100 W 13.56 MHz	3 Torr	C_2H_4/H_2 (5~20/95~80)	100 sccm	50~200W 13.56MHz	600~1000 °C	SEM, TEM	-	Tip-growth is main mechanism for CNFs; bias-power plays important role in the CNF growth.	[19]
11	100~300W 13.56 MHz	1 Torr	CH_4/H_2 (50/50)	120 sccm	-	500~650 °C	micro-Raman spectra	-	SWCNTs were grown under low ICP power	[20, 21]
12,18	1800~3000 W 0.46 MHz	20~70 mTorr	$Ar/CH_4/H_2$ (69/17/12)	20~70 sccm	-500~40V DC	300~500 °C	QMS, OES and Global modelling	n_e~10^{12} cm^{-3} T_{eff}~3.5 eV	A very efficient dissociation of hydrocarbon and molecular hydrogen feedstock is observed. H_2, CH_3, CH_4, C_2H_2, C_2H_4 are found to be the main neutral species	[22, 30]
13	1000W 13.56 MHz	50 mTorr	C_2H_2/H_2 (37.5~88/62.5~12)	50~200 sccm	-200V (27W) 13.56MHz	700 °C	OES	H, CH, CH^+, C_2 were detected	Plasma conditions change the CNF structure	[23]
14	250~1000W 13.56 MHz	20 mTorr	C_2H_2/H_2 (15/85)	20 sccm	400W 13.56 MHz	500 °C	OES	H, CH, C_2 were studied	The C_2 line intensity increases with C_2H_2/H_2 ratio, while the H atom intensity decreases	[24]
15	500~1800 W 13.56 MHz	17 mTorr	C_2H_2/H_2 (25/75)	32 sccm	-400V DC	550~650 °C	OES and MS	-	Long chain hydrocarbon produced with acetylene in the plasma	[25]
19	100W 13.56 MHz	1~7 Torr/ 100mTorr	$C_2H_2/H_2/Ar$ (40/10/50)	-	-50V DC	300 K	2D fluid simulation	T_e=1.2~3.3 eV	Ar^+, H, CH, C_2, CH_3 suggested as main species	[31]

Table 3. Different species considered in the CH_4/H_2 model, besides electrons

Molecules	Ions	Radicals
H_2	H^+, H_2^+, H_3^+	H
CH_4	C^+, CH^+, CH_2^+, CH_3^+, CH_4^+,CH_5^+	C, CH, CH_2, CH_3
C_2H_2, C_2H_4, C_2H_6	C_2^+, C_2H^+, $C_2H_2^+$, $C_2H_3^+$, $C_2H_4^+$, $C_2H_5^+$, $C_2H_6^+$	C_2, C_2H, C_2H_3, C_2H_5
C_3H_8, C_4H_{10}		

Table 4. Electron impact collisions included in the CH_4/H_2 model and their corresponding threshold energies, and references where the cross sections were adopted from.

No	Reaction	Threshold Energy(eV)	Reaction Type	Reference
	H_2			
1	$e^- + H_2 \rightarrow H_2 + e^-$	0.0	Momentum transfer	[56]
2	$e^- + H_2^{(j=0)} \rightarrow H_2^{(j=2)} + e^-$	0.044	Rotational excitation	[56]
3	$e^- + H_2^{(j=1)} \rightarrow H_2^{(j=3)} + e^-$	0.073	Rotational excitation	[56]
4	$e^- + H_2^{(v=0)} \rightarrow H_2^{(v=1)} + e^-$	0.516	Vibrational excitation	[56]
5	$e^- + H_2^{(v=0)} \rightarrow H_2^{(v=2)} + e^-$	1.000	Vibrational excitation	[56]
6	$e^- + H_2^{(v=0)} \rightarrow H_2^{(v=3)} + e^-$	1.500	Vibrational excitation	[56]
7	$e^- + H_2 \rightarrow H_2\,(b3) + e^-$	8.900	Electronic excitation	[56]
8	$e^- + H_2 \rightarrow H_2\,(B1) + e^-$	11.300	Electronic excitation	[56]
9	$e^- + H_2 \rightarrow H_2\,(c3) + e^-$	11.75	Electronic excitation	[56]
10	$e^- + H_2 \rightarrow H_2\,(a3) + e^-$	11.800	Electronic excitation	[56]
11	$e^- + H_2 \rightarrow H_2\,(C1) + e^-$	12.400	Electronic excitation	[56]
12	$e^- + H_2 \rightarrow H_2\,(d3) + e^-$	14.000	Electronic excitation	[56]
13	$e^- + H_2 \rightarrow H + H + e^-$	8.870	Dissociation	[56]
14	$e^- + H_2 \rightarrow H_2^+ + 2e^-$	15.400	Ionization	[56]
15	$e^- + H_2^+ \rightarrow H + H$	0.0	Recombination	[57]
	CH_4			
16	$e^- + CH_4 \rightarrow CH_4 + e^-$	0.000	Momentum transfer	[58, 59]
17	$e^- + CH_4^{(v=1)} \rightarrow CH_4^{(v=3)} + e^-$	0.3839	Vibrational excitation	[58, 59]
18	$e^- + CH_4^{(v=2)} + e^- \rightarrow CH_4^{(v=4)} + e^-$	0.1649	Vibrational excitation	[58, 59]
19	$e^- + CH_4 \rightarrow CH_3 + H + e^-$	8.800	Dissociation	[60]
20	$e^- + CH_4 \rightarrow CH_2 + H_2 + e^-$	9.400	Dissociation	[60]
21	$e^- + CH_4 \rightarrow CH + H_2 + H + e^-$	12.50	Dissociation	[60]
22	$e^- + CH_4 \rightarrow C + H_2 + H_2 + e^-$	14.00	Dissociation	[60]
23	$e^- + CH_4 \rightarrow CH_4^+ + 2e^-$	12.63	Ionization	[61]
24	$e^- + CH_4 \rightarrow CH_3^+ + H + 2e^-$	14.01	Dissociative ionization	[61]
	CH_3			
25	$e^- + CH_3 \rightarrow CH_3 + e^-$	0.000	Momentum transfer	[62]
26	$e^- + CH_3 \rightarrow CH_2 + H + e^-$	9.500	Dissociation	[62]
27	$e^- + CH_3 \rightarrow CH + H_2 + e^-$	10.000	Dissociation	[62]
28	$e^- + CH_3 \rightarrow CH_3^+ + 2e^-$	9.800	Ionization	[62]
	C_2H_6			
29	$e^- + C_2H_6 \rightarrow C_2H_6 + e^-$	0.000	Momentum transfer	[63]
30	$e^- + C_2H_6^{(0)} \rightarrow C_2H_6^{(v=1)} + e^-$	0.3766	Vibrational excitation	[63]
31	$e^- + C_2H_6^{(0)} \rightarrow C_2H_6^{(v=2)} + e^-$	0.1569	Vibrational excitation	[63]
32	$e^- + C_2H_6^{(0)} \rightarrow C_2H_6^{(v=3)} + e^-$	0.1099	Vibrational excitation	[63]
33	$e^- + C_2H_6 \rightarrow C_2H_5 + H + e^-$	7.45	Dissociation	[63]
34	$e^- + C_2H_6 \rightarrow C_2H_4 + H_2 + e^-$	4.00	Dissociation	[63]
35	$e^- + C_2H_6 \rightarrow C_2H_6^+ + 2e^-$	11.60	Ionization	[63]
36	$e^- + C_2H_6 \rightarrow C_2H_5^+ + H + 2e^-$	12.65	Dissociative ionization	[63]
37	$e^- + C_2H_6 \rightarrow C_2H_4^+ + H_2 + 2e^-$	11.81	Dissociative ionization	[63]
	C_2H_4			
38	$e^- + C_2H_4 \rightarrow C_2H_4 + e^-$	0.000	Momentum transfer	[63]
39	$e^- + C_2H_4^{(0)} \rightarrow C_2H_4^{(v=1)} + e^-$	0.3838	Vibrational excitation	[63]
40	$e^- + C_2H_4^{(0)} \rightarrow C_2H_4^{(v=4)} + e^-$	0.1197	Vibrational excitation	[63]
41	$e^- + C_2H_4 \rightarrow C_2H_3 + H + e^-$	6.90	Dissociation	[63]
42	$e^- + C_2H_4 \rightarrow C_2H_2 + H_2 + e^-$	5.80	Dissociation	[63]
43	$e^- + C_2H_4 \rightarrow C_2H_4^+ + 2e^-$	11.00	Ionization	[63]
44	$e^- + C_2H_4 \rightarrow C_2H_3^+ + H + 2e^-$	12.60	Dissociative ionization	[63]

45	$e^- + C_2H_4 \rightarrow C_2H_2^+ + H_2 + 2e^-$	14.30	Dissociative ionization	[63]
	C_2H_2			
46	$e^- + C_2H_2 \rightarrow C_2H_2 + e^-$	0.000	Momentum transfer	[63]
47	$e^- + C_2H_2\ ^{(0)} \rightarrow C_2H_2^{(v=1)} + e^-$	0.09	Vibrational excitation	[64]
48	$e^- + C_2H_2\ ^{(0)} \rightarrow C_2H_2^{(v=2)} + e^-$	0.29	Vibrational excitation	[64]
49	$e^- + C_2H_2\ ^{(0)} \rightarrow C_2H_2^{(v=3)} + e^-$	0.41	Vibrational excitation	[64]
50	$e^- + C_2H_2 \rightarrow C_2H + H + e^-$	7.5	Dissociation	[65]
51	$e^- + C_2H_2 \rightarrow C_2H_2^+ + 2e^-$	11.40	Ionization	[65]
52	$e^- + C_2H_2 \rightarrow C_2H^+ + H + 2e^-$	16.5	Dissociative ionization	[65]
	C_3H_8			
53	$e^- + C_3H_8 \rightarrow C_3H_8 + e^-$	0.0	Momentum transfer	[63]
54	$e^- + C_3H_8\ ^{(0)} \rightarrow C_3H_8^{(v=1)} + e^-$	0.0961	Vibrational excitation	[63]
55	$e^- + C_3H_8\ ^{(0} \rightarrow C_3H_8^{(v=2)} + e^-$	0.3593	Vibrational excitation	[63]
56	$e^- + C_3H_8 \rightarrow C_2H_5^+ + CH_3 + 2e^-$	13.92	Dissociative ionization	[63]
57	$e^- + C_3H_8 \rightarrow C_2H_4^+ + CH_4 + 2e^-$	14.19	Dissociative ionization	[63]
58	$e^- + C_3H_8 \rightarrow C_2H_4 + CH_4 + e^-$	2.1	Dissociation	[63]

Table 5. Ion-molecule reactions taken into account in the CH_4/H_2 model, as well as their reaction rate coefficients. The latter were all adopted from [66].

No.	Reaction	Coefficient(cm^3s^{-1})
1	$H^+ + H_2 \rightarrow H_2^+ + H$	$3.22\times10^{-10}\times\exp(21856/T)$
2	$H^+ + CH \rightarrow CH^+ + H$	1.89×10^{-9}
3	$H^+ + CH_2 \rightarrow CH^+ + H_2$	1.39×10^{-9}
4	$H^+ + CH_2 \rightarrow CH_2^+ + H$	1.39×10^{-9}
5	$H^+ + CH_3 \rightarrow CH_3^+ + H$	3.32×10^{-9}
6	$H^+ + CH_4 \rightarrow CH_3^+ + H_2$	2.33×10^{-9}
7	$H^+ + C_2 \rightarrow C_2^+ + H$	3.09×10^{-9}
8	$H^+ + C_2H \rightarrow C_2^+ + H_2$	1.50×10^{-9}
9	$H^+ + C_2H \rightarrow C_2H^+ + H$	1.50×10^{-9}
10	$H^+ + C_2H_2 \rightarrow C_2H^+ + H_2$	2.00×10^{-9}
11	$H^+ + C_2H_2 \rightarrow C_2H_2^+ + H$	2.00×10^{-9}
12	$H^+ + C_2H_3 \rightarrow C_2H_2^+ + H_2$	2.00×10^{-9}
13	$H^+ + C_2H_3 \rightarrow C_2H_3^+ + H$	2.00×10^{-9}
14	$H^+ + C_2H_4 \rightarrow C_2H_2^+ + H_2 + H$	1.00×10^{-9}
15	$H^+ + C_2H_4 \rightarrow C_2H_4^+ + H$	1.00×10^{-9}
16	$H^+ + C_2H_4 \rightarrow C_2H_3^+ + H_2$	3.00×10^{-9}
17	$H^+ + C_2H_5 \rightarrow C_2H_3^+ + H_2 + H$	3.06×10^{-9}
18	$H^+ + C_2H_5 \rightarrow C_2H_4^+ + H_2$	1.65×10^{-9}
19	$H_2^+ + H \rightarrow H^+ + H_2$	6.40×10^{-10}
19	$H_2^+ + H_2 \rightarrow H_3^+ + H$	2.08×10^{-9}
20	$H_2^+ + C \rightarrow CH^+ + H$	2.40×10^{-9}
21	$H_2^+ + CH \rightarrow CH^+ + H_2$	7.10×10^{-10}
22	$H_2^+ + CH \rightarrow CH_2^+ + H$	7.10×10^{-10}
23	$H_2^+ + CH_2 \rightarrow CH_3^+ + H$	1.00×10^{-9}
24	$H_2^+ + CH_2 \rightarrow CH_2^+ + H_2$	1.00×10^{-9}
25	$H_2^+ + CH_4 \rightarrow CH_5^+ + H$	1.14×10^{-10}
26	$H_2^+ + CH_4 \rightarrow CH_4^+ + H_2$	1.40×10^{-9}
27	$H_2^+ + CH_4 \rightarrow CH_3^+ + H_2 + H$	2.30×10^{-9}
28	$H_2^+ + C_2 \rightarrow C_2^+ + H_2$	1.10×10^{-9}
29	$H_2^+ + C_2 \rightarrow C_2H^+ + H$	1.10×10^{-9}
30	$H_2^+ + C_2H \rightarrow C_2H^+ + H_2$	1.00×10^{-9}
31	$H_2^+ + C_2H \rightarrow C_2H_2^+ + H$	1.00×10^{-9}
32	$H_2^+ + C_2H_2 \rightarrow C_2H_3^+ + H$	4.80×10^{-10}
33	$H_2^+ + C_2H_2 \rightarrow C_2H_2^+ + H_2$	4.82×10^{-9}
34	$H_2^+ + C_2H_4 \rightarrow C_2H_3^+ + H_2 + H$	1.81×10^{-9}
35	$H_2^+ + C_2H_4 \rightarrow C_2H_4^+ + H_2$	2.21×10^{-9}
36	$H_2^+ + C_2H_4 \rightarrow C_2H_2^+ + H_2 + H_2$	8.82×10^{-9}
37	$H_3^+ + C \rightarrow CH^+ + H_2$	2.00×10^{-9}
38	$H_3^+ + CH \rightarrow CH_2^+ + H_2$	1.20×10^{-9}
39	$H_3^+ + CH_2 \rightarrow CH_3^+ + H_2$	1.70×10^{-9}
40	$H_3^+ + CH_3 \rightarrow CH_4^+ + H_2$	2.10×10^{-9}
41	$H_3^+ + CH_4 \rightarrow CH_5^+ + H_2$	2.40×10^{-9}
42	$H_3^+ + C_2 \rightarrow C_2H^+ + H_2$	1.80×10^{-9}
43	$H_3^+ + C_2H \rightarrow C_2H_2^+ + H_2$	1.70×10^{-9}
44	$H_3^+ + C_2H_2 \rightarrow C_2H_3^+ + H_2$	3.50×10^{-9}
45	$H_3^+ + C_2H_3 \rightarrow C_2H_4^+ + H_2$	2.00×10^{-9}
46	$H_3^+ + C_2H_4 \rightarrow C_2H_5^+ + H_2$	1.15×10^{-9}
47	$H_3^+ + C_2H_4 \rightarrow C_2H_3^+ + H_2 + H_2$	1.15×10^{-9}
48	$H_3^+ + C_2H_5 \rightarrow C_2H_6^+ + H_2$	1.40×10^{-9}
49	$C^+ + CH \rightarrow C_2^+ + H$	3.82×10^{-10}

50	$C^+ + CH \rightarrow CH^+ + C$	3.82×10^{-10}
51	$C^+ + CH_2 \rightarrow C_2H^+ + H$	5.15×10^{-10}
52	$C^+ + CH_2 \rightarrow CH_2^+ + C$	5.15×10^{-10}
53	$C^+ + CH_4 \rightarrow C_2H_2^+ + H_2$	3.16×10^{-10}
54	$C^+ + CH_4 \rightarrow C_2H_3^+ + H$	9.63×10^{-10}
55	$C^+ + C_2H_4 \rightarrow C_2H_3^+ + CH$	8.50×10^{-11}
56	$C^+ + C_2H_4 \rightarrow C_2H_4^+ + C$	1.70×10^{-11}
57	$C^+ + C_2H_5 \rightarrow C_2H_5^+ + C$	5.00×10^{-10}
58	$CH^+ + H \rightarrow C^+ + H_2$	7.50×10^{-10}
59	$CH^+ + H_2 \rightarrow CH_2^+ + H$	1.20×10^{-9}
60	$CH^+ + C \rightarrow C_2^+ + H$	1.20×10^{-9}
61	$CH^+ + CH \rightarrow C_2^+ + H_2$	1.00×10^{-9}
62	$CH^+ + CH_2 \rightarrow C_2H^+ + H_2$	7.50×10^{-10}
63	$CH^+ + CH_4 \rightarrow C_2H_2^+ + H_2 + H$	1.43×10^{-10}
64	$CH^+ + CH_4 \rightarrow C_2H_4^+ + H$	6.50×10^{-11}
65	$CH^+ + CH_4 \rightarrow C_2H_3^+ + H_2$	1.09×10^{-9}
66	$CH_2^+ + H \rightarrow CH^+ + H_2$	1.00×10^{-9}
67	$CH_2^+ + H_2 \rightarrow CH_3^+ + H$	1.60×10^{-9}
68	$CH_2^+ + C \rightarrow C_2H^+ + H$	1.20×10^{-9}
69	$CH_2^+ + CH_4 \rightarrow C_2H_4^+ + H_2$	8.40×10^{-10}
70	$CH_2^+ + CH_4 \rightarrow C_2H_5^+ + H$	3.60×10^{-10}
71	$CH_3^+ + H \rightarrow CH_2^+ + H_2$	7.00×10^{-10}
72	$CH_3^+ + C \rightarrow C_2H^+ + H_2$	1.20×10^{-9}
73	$CH_2^+ + CH \rightarrow C_2H_2^+ + H_2$	7.10×10^{-10}
74	$CH_2^+ + CH_2 \rightarrow C_2H_3^+ + H_2$	9.90×10^{-10}
75	$CH_3^+ + CH_4 \rightarrow C_2H_5^+ + H_2$	1.20×10^{-9}
76	$CH_3^+ + C_2H_3 \rightarrow C_2H_3^+ + CH_3$	3.00×10^{-10}
77	$CH_3^+ + C_2H_4 \rightarrow C_2H_3^+ + CH_4$	3.50×10^{-10}
78	$CH_4^+ + H \rightarrow CH_3^+ + H_2$	1.10×10^{-11}
79	$CH_4^+ + H_2 \rightarrow CH_5^+ + H$	3.30×10^{-11}
80	$CH_4^+ + CH_4 \rightarrow CH_5^+ + CH_3$	1.50×10^{-9}
81	$CH_4^+ + C_2H_2 \rightarrow C_2H_2^+ + CH_4$	1.13×10^{-9}
82	$CH_4^+ + C_2H_2 \rightarrow C_2H_3^+ + CH_3$	1.23×10^{-9}
83	$CH_4^+ + C_2H_4 \rightarrow C_2H_4^+ + CH_4$	1.38×10^{-9}
84	$CH_4^+ + C_2H_4 \rightarrow C_2H_5^+ + CH_3$	4.23×10^{-10}
85	$CH_5^+ + H \rightarrow CH_4^+ + H_2$	1.50×10^{-10}
86	$CH_5^+ + C \rightarrow CH^+ + CH_4$	1.20×10^{-9}
87	$CH_5^+ + CH \rightarrow CH_2^+ + CH_4$	6.90×10^{-10}
88	$CH_5^+ + CH_2 \rightarrow CH_3^+ + CH_4$	9.60×10^{-10}
89	$CH_5^+ + C_2 \rightarrow C_2H^+ + CH_4$	9.50×10^{-10}
90	$CH_5^+ + C_2H \rightarrow C_2H_2^+ + CH_4$	9.00×10^{-10}
91	$CH_5^+ + C_2H_2 \rightarrow C_2H_3^+ + CH_4$	1.60×10^{-9}
92	$CH_5^+ + C_2H_4 \rightarrow C_2H_5^+ + CH_4$	1.50×10^{-9}
93	$C_2^+ + H_2 \rightarrow C_2H^+ + H$	1.10×10^{-9}
94	$C_2^+ + C \rightarrow C^+ + C_2$	1.10×10^{-10}
95	$C_2^+ + CH \rightarrow CH^+ + C_2$	3.20×10^{-10}
96	$C_2^+ + CH_2 \rightarrow CH_2^+ + C_2$	4.50×10^{-10}
97	$C_2^+ + CH_4 \rightarrow C_2H^+ + CH_3$	2.38×10^{-10}
98	$C_2^+ + CH_4 \rightarrow C_2H_2^+ + CH_2$	1.82×10^{-10}
99	$C_2H^+ + H_2 \rightarrow C_2H_2^+ + H$	1.10×10^{-9}
100	$C_2H^+ + CH \rightarrow CH_2^+ + C_2$	3.20×10^{-10}
101	$C_2H^+ + CH_2 \rightarrow CH_3^+ + C_2$	4.40×10^{-10}
102	$C_2H^+ + CH_4 \rightarrow C_2H_2^+ + CH_3$	3.74×10^{-10}
103	$C_2H_2^+ + H_2 \rightarrow C_2H_3^+ + H$	1.00×10^{-11}
104	$C_2H_2^+ + C_2H_3 \rightarrow C_2H_3^+ + C_2H_2$	3.30×10^{-10}

105	$C_2H_2^+ + C_2H_4 \rightarrow C_2H_4^+ + C_2H_2$	4.14×10^{-10}
106	$C_2H_3^+ + H \rightarrow C_2H_2^+ + H_2$	6.80×10^{-11}
107	$C_2H_3^+ + C_2H \rightarrow C_2H_2^+ + C_2H_2$	3.30×10^{-10}
108	$C_2H_3^+ + C_2H_3 \rightarrow C_2H_5^+ + C_2H$	5.00×10^{-10}
109	$C_2H_3^+ + C_2H_4 \rightarrow C_2H_5^+ + C_2H_2$	8.90×10^{-10}
110	$C_2H_4^+ + H \rightarrow C_2H_3^+ + H_2$	3.00×10^{-10}
111	$C_2H_4^+ + C_2H_3 \rightarrow C_2H_3^+ + C_2H_4$	5.00×10^{-10}
112	$C_2H_4^+ + C_2H_3 \rightarrow C_2H_5^+ + C_2H_2$	5.00×10^{-10}
113	$C_2H_5^+ + H \rightarrow C_2H_4^+ + H_2$	1.00×10^{-11}
114	$C_2H_6^+ + H \rightarrow C_2H_5^+ + H_2$	1.00×10^{-10}
115	$C_2H_6^+ + C_2H_2 \rightarrow C_2H_5^+ + C_2H_3$	2.47×10^{-10}

Table 6. Neutral-neutral reactions taken into account in the CH_4/H_2 model. The rate coefficients are calculated by $k=k_0\times(T_g/298)^n\times\exp(-E_a/T_g)$, where T_g is the gas temperature (K). The parameters k_0, n, and E_a are given in the table; they were all adopted from [30, 67, 68].

No.	Reactions	Rate coefficient		
		$k_0(cm^3s^{-1})$	n	E_a/R
1	$H + H + M \rightarrow H_2 + M$	1.90×10^{-31}	-0.06	0
2	$CH_4 + CH_3 \rightarrow C_2H_5 + H_2$	1.70×10^{-11}	0	11500
3	$CH_4 + CH_2 \rightarrow CH_3 + CH_3$	7.10×10^{-12}	0	5020
4	$CH_4 + CH_2 \rightarrow C_2H_4 + H_2$	1.70×10^{-11}	0	0
5	$CH_4 + CH \rightarrow C_2H_5$	1.00×10^{-10}	0	0
6	$CH_4 + CH \rightarrow C_2H_4 + H$	5.00×10^{-11}	0	-200
7	$CH_4 + C_2H_3 \rightarrow C_2H_4 + CH_2$	1.89×10^{-14}	4.0	2754
8	$CH_4 + C_2H \rightarrow C_2H_2 + CH_3$	3.00×10^{-12}	0	250
9	$CH_4 + H \rightarrow CH_3 + H_2$	5.82×10^{-13}	3.0	4045
10	$CH_3 + CH_3 \rightarrow C_2H_6$	4.10×10^{-11}	-0.4	0
11	$CH_3 + CH_3 \rightarrow C_2H_5 + H$	5.00×10^{-11}	0	6800
12	$CH_3 + CH_3 \rightarrow C_2H_4 + H_2$	1.70×10^{-08}	0	16000
13	$CH_3 + CH_2 \rightarrow C_2H_4 + H$	7.00×10^{-11}	0	0
14	$CH_3 + CH \rightarrow C_2H_3 + H$	5.00×10^{-11}	0	0
15	$CH_3 + C \rightarrow C_2H_2 + H$	8.30×10^{-11}	0	0
16	$CH_3 + H \rightarrow CH_4$	7.00×10^{-12}	0	0
17	$CH_3 + H \rightarrow CH_2 + H_2$	1.00×10^{-10}	0	7600
18	$CH_3 + C_2H_5 \rightarrow C_2H_4 + CH_4$	1.90×10^{-12}	0	0
19	$CH_3 + C_2H_5 \rightarrow C_3H_8$	4.70×10^{-11}	0	0
20	$CH_3 + C_2H_3 \rightarrow C_2H_2 + CH_4$	6.50×10^{-14}	0	0
21	$CH_2 + CH_2 \rightarrow C_2H_4$	1.70×10^{-12}	0	0
22	$CH_2 + CH_2 \rightarrow C_2H_2 + H + H$	1.80×10^{-10}	0	400
23	$CH_2 + CH_2 \rightarrow C_2H_2 + H_2$	2.00×10^{-11}	0	400
24	$CH_2 + CH \rightarrow C_2H_2 + H$	6.60×10^{-11}	0	0
25	$CH_2 + C \rightarrow C_2H + H$	8.30×10^{-11}	0	0
26	$CH_2 + H \rightarrow CH + H_2$	7.70×10^{-10}	0	0
27	$CH_2 + C_2H_3 \rightarrow C_2H_2 + CH_3$	3.00×10^{-11}	0	0
28	$CH_2 + C_2H \rightarrow C_2H_2 + CH$	3.00×10^{-11}	0	0
29	$CH + CH \rightarrow C_2H_2$	2.00×10^{-10}	0	0
30	$C_2H_5 + C_2H_5 \rightarrow C_2H_6 + C_2H_4$	2.40×10^{-12}	0	0
31	$C_2H_5 + C_2H_5 \rightarrow C_4H_{10}$	1.90×10^{-11}	0	0
32	$C_2H_5 + C_2H_3 \rightarrow C_2H_6 + C_2H_2$	8.00×10^{-13}	0	0
33	$C_2H_5 + C_2H_3 \rightarrow C_2H_4 + C_2H_4$	8.00×10^{-13}	0	0
34	$C_2H_5 + C_2H \rightarrow C_2H_4 + C_2H_2$	3.00×10^{-12}	0	0
35	$C_2H_5 + H \rightarrow C_2H_6$	6.00×10^{-11}	0	0
36	$C_2H_5 + H \rightarrow CH_3 + CH_3$	6.00×10^{-11}	0	0
37	$C_2H_5 + H \rightarrow C_2H_4 + H_2$	3.00×10^{-12}	0	0
38	$C_2H_3 + H \rightarrow C_2H_2 + H_2$	2.00×10^{-11}	0	0
39	$C_2H_6 + CH_3 \rightarrow C_2H_5 + CH_4$	1.75×10^{-16}	6	3043
40	$C_2H_6 + C_2H \rightarrow C_2H_2 + C_2H_5$	6.00×10^{-12}	0	0
41	$C_2H_6 + H \rightarrow C_2H_5 + H_2$	1.23×10^{-11}	1.5	3730
42	$C_2H_2 + H \rightarrow C_2H + H_2$	1.00×10^{-10}	0	0
43	$C_2H_4 + H \rightarrow C_2H_3 + H_2$	9.00×10^{-10}	0	0
44	$CH_2 + C_2H_6 \rightarrow C_3H_8$	4.00×10^{-10}	0	0
45	$CH_2 + C_3H_8 \rightarrow C_4H_{10}$	1.89×10^{-12}	0	0

Table 7. Different species considered in the C_2H_2/H_2 model, besides electrons

Molecules	Ions	Radicals
H_2	H^+, H_2^+,	H
C_2H_2	$C_2H_2^+$, C_2H^+, CH^+, CH_2^+, C_2^+, C^+	C, CH, CH_2, C_2, C_2H
C_4H_2, C_6H_2, C_8H_2, $C_{10}H_2$, $C_{12}H_2$	C_4H^+, C_6H^+, C_8H^+, $C_4H_2^+$, $C_6H_2^+$, $C_8H_2^+$	C_4H, C_6H, C_8H, $C_{10}H$, $C_{12}H$
	$C_2H_3^+$, $C_4H_3^+$	C_2H_3, C_4H_3, C_6H_3
C_6H_4, C_8H_4, C_8H_6, $C_{10}H_6$, $C_{12}H_6$	$C_6H_4^+$, $C_8H_4^+$, $C_8H_6^+$, $C_{10}H_6^+$, $C_{12}H_6^+$	

Table 8. Electron impact collisions included in the C_2H_2/H_2 model and their corresponding threshold energies, and the references where the cross sections are adopted from.

No.	Reaction	Threshold Energy(eV)	Reaction Type	Reference
1	$C_2H_2 + e^- \rightarrow C_2H_2^+ + 2e^-$	11.4	Ionization	[65]
2	$C_2H_2 + e^- \rightarrow C_2H^+ + H + 2e^-$	16.5	Dissociative ionization	[65]
3	$C_2H_2 + e^- \rightarrow C_2^+ + H_2 + 2e^-$	17.5	Dissociative ionization	[65]
4	$C_2H_2 + e^- \rightarrow CH^+ + CH + 2e^-$	20.6	Dissociative ionization	[65]
5	$C_2H_2 + e^- \rightarrow C^+ + CH_2 + 2e^-$	20.3	Dissociative ionization	[65]
6	$C_2H_2 + e^- \rightarrow H^+ + C_2H + 2e^-$	18.4	Dissociative ionization	[65]
7	$C_2H_2\ ^{(0)} + e^- \rightarrow C_2H_2^{(v=5)} + e^-$	0.09	Vibrational excitation	[64]
8	$C_2H_2\ ^{(0)} + e^- \rightarrow C_2H_2^{(v=2)} + e^-$	0.29	Vibrational excitation	[64]
9	$C_2H_2\ ^{(0)} + e^- \rightarrow C_2H_2^{(v=3)} + e^-$	0.41	Vibrational excitation	[64]
10	$C_2H_2 + e^- \rightarrow C_2H + H + e^-$	7.5	Dissociation	[65]
11	$H_2 + e^- \rightarrow H_2 + e^-$	0.0	Momentum transfer	[56]
12	$H_2\ ^{(j=0)} + e^- \rightarrow H_2\ ^{(j=2)} + e^-$	0.044	Rotational excitation	[56]
13	$H_2\ ^{(j=1)} + e^- \rightarrow H_2\ ^{(j=3)} + e^-$	0.073	Rotational excitation	[56]
14	$H_2\ ^{(v=0)} + e^- \rightarrow H_2\ ^{(v=1)} + e^-$	0.516	Vibrational excitation	[56]
15	$H_2\ ^{(v=0)} + e^- \rightarrow H_2\ ^{(v=2)} + e^-$	1.000	Vibrational excitation	[56]
16	$H_2\ ^{(v=0)} + e^- \rightarrow H_2\ ^{(v=3)} + e^-$	1.500	Vibrational excitation	[56]
17	$H_2 + e^- \rightarrow H_2\ (b3) + e^-$	8.900	Electronic excitation	[56]
18	$H_2 + e^- \rightarrow H_2\ (B1) + e^-$	11.300	Electronic excitation	[56]
19	$H_2 + e^- \rightarrow H_2\ (c3) + e^-$	11.75	Electronic excitation	[56]
20	$H_2 + e^- \rightarrow H_2\ (a3) + e^-$	11.800	Electronic excitation	[56]
21	$H_2 + e^- \rightarrow H_2\ (C1) + e^-$	12.400	Electronic excitation	[56]
22	$H_2 + e^- \rightarrow H_2\ (d3) + e^-$	14.000	Electronic excitation	[56]
23	$H_2 + e^- \rightarrow H + H + e^-$	8.870	Dissociation	[56]
24	$H_2 + e^- \rightarrow H_2^+ + 2e^-$	15.400	Ionization	[56]
25	$C_4H_2 + e^- \rightarrow C_4H + H + e^-$	7.5	Dissociation	[65]
26	$C_6H_2 + e^- \rightarrow C_6H + H + e^-$	7.5	Dissociation	[65]
27	$C_8H_2 + e^- \rightarrow C_8H + H + e^-$	7.5	Dissociation	[65]
28	$C_{10}H_2 + e^- \rightarrow C_{10}H + H + e^-$	7.5	Dissociation	[65]
29	$C_{12}H_2 + e^- \rightarrow C_{12}H + H + e^-$	7.5	Dissociation	[65]
30	$C_4H_2 + e^- \rightarrow C_4H_2^+ + 2e^-$	10.19	Ionization	[69]
31	$C_6H_2 + e^- \rightarrow C_6H_2^+ + 2e^-$	9.55	Ionization	[69]

Table 9. Ion-molecule reactions taken into account in the C_2H_2/H_2 model, as well as their reaction rate coefficients. The latter were all adopted from [66].

No	Reaction	Coefficient(cm^3s^{-1})
1	$H^+ + C_2 \rightarrow C_2^+ + H$	3.10×10^{-9}
2	$H^+ + C_4H \rightarrow C_4H^+ + H$	2.00×10^{-9}
3	$H^+ + C_6H \rightarrow C_6H^+ + H$	2.00×10^{-9}
4	$H^+ + C_8H \rightarrow C_8H^+ + H$	2.00×10^{-9}
5	$H^+ + C_2H_2 \rightarrow C_2H^+ + H_2$	4.30×10^{-9}
6	$H^+ + C_4H_2 \rightarrow C_4H^+ + H_2$	2.00×10^{-9}
7	$H^+ + C_8H_2 \rightarrow C_8H^+ + H_2$	2.00×10^{-9}
8	$H_2^+ + H \rightarrow H^+ + H_2$	6.40×10^{-10}
9	$H_2^+ + C_2 \rightarrow C_2^+ + H_2$	1.10×10^{-9}
10	$H_2^+ + C_2H_2 \rightarrow C_2H_2^+ + H_2$	5.30×10^{-9}
11	$H_2^+ + C_4H \rightarrow C_4H_2^+ + H$	1.70×10^{-10}
12	$H_2 + C_2H^+ \rightarrow C_2H_2^+ + H$	1.70×10^{-9}
13	$H_2 + C_8H^+ \rightarrow C_8H_2^+ + H$	1.00×10^{-9}
14	$C_2H + C_4H^+ \rightarrow C_6H^+ + H$	6.00×10^{-10}
15	$C_2H + C_4H_2^+ \rightarrow C_6H_2^+ + H$	1.30×10^{-9}
16	$C_2H + C_6H_2^+ \rightarrow C_8H_2^+ + H$	1.20×10^{-9}
17	$C_2H_2 + C_2^+ \rightarrow C_4H^+ + H$	1.70×10^{-9}
18	$C_2H_2 + C_2H^+ \rightarrow C_4H_2^+ + H$	1.20×10^{-9}
19	$C_2H_2 + C_2H_3^+ \rightarrow C_4H_3^+ + H_2$	2.40×10^{-10}
20	$C_2H_2 + C_4H^+ \rightarrow C_6H_2^+ + H$	1.50×10^{-9}
21	$C_2H_2 + C_4H_2^+ \rightarrow C_6H_4^+$	1.40×10^{-10}
22	$C_2H_2 + C_2H_2^+ \rightarrow C_4H_3^+ + H$	9.50×10^{-10}
23	$C_2H_2 + C_2H_2^+ \rightarrow C_4H_2^+ + H_2$	1.20×10^{-9}
24	$C_2H_2 + C_6H_4^+ \rightarrow C_8H_6^+$	1.00×10^{-10}
25	$C_2H_2 + C_8H_4^+ \rightarrow C_{10}H_6^+$	5.00×10^{-11}
26	$C_2H_2 + C_8H_6^+ \rightarrow C_{10}H_6^+ + H_2$	5.00×10^{-11}
27	$C_2H_2 + C_{10}H_6^+ \rightarrow C_{12}H_6^+ + H_2$	1.00×10^{-11}
28	$C_2H_2 + C_6H_2^+ \rightarrow C_8H_4^+$	1.00×10^{-11}
29	$C_2H_2 + C_6H_2^+ \rightarrow C_8H_2^+ + H_2$	1.00×10^{-11}
30	$C_2H_2^+ + H_2 \rightarrow C_2H_3^+ + H$	1.00×10^{-11}
31	$C_2H_2^+ + C_6H_2 \rightarrow C_8H_2^+ + H_2$	5.00×10^{-10}
32	$C_2H_2^+ + C_6H \rightarrow C_8H_2^+ + H$	1.20×10^{-9}
33	$C_2H_2^+ + C_6H_2 \rightarrow C_6H_2^+ + C_2H_2$	5.00×10^{-10}
34	$C_2H_2^+ + C_6H \rightarrow C_8H^+ + H_2$	1.20×10^{-09}

35	$C_2H_3 + C_2H_2^+ \rightarrow C_4H_3^+ + H_2$	3.30×10^{-10}
36	$C_2H_3 + C_4H_2^+ \rightarrow C_6H_4^+ + H$	1.20×10^{-9}
37	$C_2H_3 + C_4H_3^+ \rightarrow C_6H_4^+ + H_2$	5.00×10^{-10}
38	$C_2H_3 + C_6H_2^+ \rightarrow C_8H_4^+ + H$	4.00×10^{-10}
39	$C_2H_3^+ + H \rightarrow C_2H_2^+ + H_2$	6.80×10^{-11}
40	$C_2H_3^+ + C_6H \rightarrow C_8H_2^+ + H_2$	5.00×10^{-10}
41	$C_2H_3^+ + C_4H \rightarrow C_6H_2^+ + H_2$	4.00×10^{-10}
42	$C_2H_3^+ + C_6H \rightarrow C_6H_2^+ + C_2H_2$	5.00×10^{-10}
43	$C_2^+ + H_2 \rightarrow C_2H^+ + H$	1.10×10^{-9}
44	$C_4H^+ + C_4H \rightarrow C_8H^+ + H$	6.00×10^{-10}
45	$C_4H^+ + C_4H_2 \rightarrow C_8H_2^+ + H$	1.50×10^{-9}

Table 10. Neutral-neutral reactions taken into account in the C_2H_2/H_2 model. The rate coefficients are calculated by $k=k_0\times(T_g/298)^n\times\exp(-E_a/RT_g)$, where T_g is the gas temperature (K). The parameters k_0, n, and E_a are given in the table, as well as the references where these data are adopted from.

No.	Reactions	Rate coefficient			Ref.
		$k_0(cm^3s^{-1})$	n	Ea/R(K)	
1	$C_2H + C_2H_2 \rightarrow C_4H_2 + H$	1.30×10^{-10}	0.0	0.0	[70]
2	$C_2H + C_4H_2 \rightarrow C_6H_2 + H$	1.30×10^{-10}	0.0	0.0	[70]
3	$C_2H + C_6H_2 \rightarrow C_8H_2 + H$	1.30×10^{-10}	0.0	0.0	[70]
4	$C_2H + C_8H_2 \rightarrow C_{10}H_2 + H$	1.30×10^{-10}	0.0	0.0	[70]
5	$C_2H + C_{10}H_2 \rightarrow C_{12}H_2 + H$	1.30×10^{-10}	0.0	0.0	[70]
6	$C_2H + C_2H_2 \rightarrow C_4H_3$	4.70×10^{-10}	-6.3	1404.0	[71]
7	$C_2H + C_4H_2 \rightarrow C_6H_3$	4.70×10^{-10}	-6.3	1404.0	[71]
8	$H + C_2H_3 \rightarrow C_2H_2 + H_2$	5.00×10^{-11}	0.0	0.0	[70]
9	$H + C_4H_3 \rightarrow C_4H_2 + H_2$	2.40×10^{-11}	0.0	0.0	[71]
10	$H + C_6H_3 \rightarrow C_6H_2 + H_2$	5.00×10^{-11}	0.0	0.0	[72]
11	$C_4H + C_2H_2 \rightarrow C_6H_2 + H$	6.60×10^{-11}	0.0	0.0	[73]
12	$C_6H + C_2H_2 \rightarrow C_8H_2 + H$	6.60×10^{-11}	0.0	0.0	[73]
13	$C_8H + C_2H_2 \rightarrow C_{10}H_2 + H$	6.60×10^{-11}	0.0	0.0	[73]
14	$C_{10}H + C_2H_2 \rightarrow C_{12}H_2 + H$	6.60×10^{-11}	0.0	0.0	[73]
15	$H + C_4H_3 \rightarrow C_2H_2 + C_2H_2$	2.91×10^{-9}	-1.6	1117.0	[71]
16	$H + C_6H_3 \rightarrow C_4H_2 + C_2H_2$	4.38×10^{-9}	-1.6	1117.0	[71]
17	$C_2H + C_2H_3 \rightarrow C_2H_2 + C_2H_2$	5.00×10^{-11}	0.0	0.0	[71]
18	$C_2H_2 + H \rightarrow C_2H_3$	1.40×10^{-11}	0.0	1300.0	[71]
19	$C_4H_2 + H \rightarrow C_4H_3$	5.31×10^{-11}	1.16	882.0	[74]
20	$C_2H + H_2 \rightarrow C_2H_2 + H$	8.95×10^{-13}	2.57	130.0	[70]
21	$C_4H + H_2 \rightarrow C_4H_2 + H$	8.95×10^{-13}	2.57	130.0	[70]
22	$C_6H + H_2 \rightarrow C_6H_2 + H$	8.95×10^{-13}	2.57	130.0	[70]
23	$C_8H + H_2 \rightarrow C_8H_2 + H$	8.95×10^{-13}	2.57	130.0	[70]
24	$C_{10}H + H_2 \rightarrow C_{10}H_2 + H$	8.95×10^{-13}	2.57	130.0	[70]
25	$C_{12}H + H_2 \rightarrow C_{12}H_2 + H$	8.95×10^{-13}	2.57	130.0	[70]
26	$CH + H_2 \rightarrow CH_2 + H$	3.75×10^{-10}	0.0	1660.0	[71]
27	$CH_2 + H \rightarrow CH + H_2$	5.30×10^{-11}	0.0	0.0	[71]
28	$CH_2 + CH \rightarrow C_2H_2 + H$	8.30×10^{-11}	0.0	0.0	[71]
29	$C_2H_3 + CH \rightarrow C_2H_2 + CH_2$	8.30×10^{-11}	0.0	0.0	[71]

Table 11. Extra species considered when ammonia is included in the gas mixture

Molecules	Ions	Radicals
NH_3	NH^+, NH_2^+, NH_3^+, NH_4^+	NH_2, NH
N_2H_2, N_2H_4		N_2H, N_2H_3
N_2	N^+, N_2^+	N, N^*, N_2^*
HCN	HCN^+	H_2CN, CN

Table 12. Extra electron impact collisions and their corresponding threshold energies, included when ammonia is used as dilution gas instead of H_2. All these cross sections are adopted from [75].

No.	Reaction	Threshold Energy (eV)	Reaction Type
1	$NH_3 + e^- \rightarrow NH_3 + e^-$	0.0	Momentum
2	$NH_3 + e^- \rightarrow NH_3 + e^-$	0.1162	Vibrational excitation
3	$NH_3 + e^- \rightarrow NH_3 + e^-$	0.196	Vibrational excitation
4	$NH_3 + e^- \rightarrow NH_3 + e^-$	0.405	Vibrational excitation
5	$NH_3 + e^- \rightarrow NH_2 + H + e^-$	5.6	Dissociation
6	$NH_3 + e^- \rightarrow NH + H + H + 2e^-$	8.9	Dissociation
7	$NH_3 + e^- \rightarrow NH_3^+ + 2e^-$	10.2	Ionization
8	$NH_3 + e^- \rightarrow NH_2^+ + H + 2e^-$	16.0	Dissociative Ionization
9	$NH_2 + e^- \rightarrow NH_2 + e^-$	0.0	Momentum
10	$NH_2 + e^- \rightarrow NH_2 + e^-$	0.1162	Vibrational excitation
11	$NH_2 + e^- \rightarrow NH_2 + e^-$	0.196	Vibrational excitation
12	$NH_2 + e^- \rightarrow NH_2 + e^-$	0.405	Vibrational excitation
13	$NH_2 + e^- \rightarrow NH + H + e^-$	5.6	Dissociation
14	$NH_2 + e^- \rightarrow N + H + H + 2e^-$	8.9	Dissociation
15	$NH_2 + e^- \rightarrow NH_2^+ + 2e^-$	11.14	Ionization
16	$NH_2 + e^- \rightarrow NH^+ + H + 2e^-$	17.60	Dissociative Ionization
17	$NH + e^- \rightarrow NH + e^-$	0.0	Momentum
18	$NH + e^- \rightarrow NH + e^-$	0.1162	Vibrational excitation
19	$NH + e^- \rightarrow NH + e^-$	0.196	Vibrational excitation
20	$NH + e^- \rightarrow NH + e^-$	0.405	Vibrational excitation
21	$NH + e^- \rightarrow N + H + e^-$	5.6	Dissociation
22	$NH + e^- \rightarrow NH^+ + 2e^-$	13.49	Ionization
23	$N_2 + e^- \rightarrow N_2 + e^-$	0	Momentum
24	$N_2 + e^- \rightarrow N_2 + e^-$	0.02	Rotational excitation
25	$N_2 + e^- \rightarrow N_2 + e^-$	1.3	Vibrational excitation
26	$N_2 + e^- \rightarrow N_2 + e^-$	1.73	Vibrational excitation
27	$N_2 + e^- \rightarrow N_2 + e^-$	1.901	Vibrational excitation
28	$N_2 + e^- \rightarrow N_2 + e^-$	2.079	Vibrational excitation
29	$N_2 + e^- \rightarrow N_2 + e^-$	2.119	Vibrational excitation
30	$N_2 + e^- \rightarrow N_2 + e^-$	2.297	Vibrational excitation
31	$N_2 + e^- \rightarrow N_2 + e^-$	2.39	Vibrational excitation
32	$N_2 + e^- \rightarrow N_2 + e^-$	2.60	Vibrational excitation
33	$N_2 + e^- \rightarrow N_2^* + e^-$	6.17	Electronic excitation
34	$N_2 + e^- \rightarrow N_2^* + e^-$	7.35	Electronic excitation
35	$N_2 + e^- \rightarrow N_2^* + e^-$	8.165	Electronic excitation
36	$N_2 + e^- \rightarrow N_2^* + e^-$	8.399	Electronic excitation
37	$N_2 + e^- \rightarrow N_2^* + e^-$	11.032	Electronic excitation
38	$N_2 + e^- \rightarrow N + N + e^-$	12.253	Dissociation
39	$N_2 + e^- \rightarrow N_2^+ + 2e^-$	15.5	Ionization

40	$N + e^- \rightarrow N + e^-$	0	Momentum
41	$N + e^- \rightarrow N^* + e^-$	2.38	Electronic excitation
42	$N + e^- \rightarrow N^* + e^-$	3.57	Electronic excitation
43	$N + e^- \rightarrow N^+ + 2e^-$	14.549	Ionization

Table 13. Extra ion-molecule reactions taken into account when ammonia is used as dilution gas, as well as their rate coefficients and references where these data are adopted from. T_g is the gas temperature (K).

No	Reaction	Coefficient(cm^3s^{-1})	Reference
1	$N_2^+ + N \rightarrow N^+ + N_2$	5.00×10^{-12}	[76]
2	$N_2^+ + N^* \rightarrow N^+ + N_2$	1.00×10^{-10}	[76]
3	$N_2^+ + N_2 \rightarrow N_2^+ + N_2$	1.00×10^{-9}	[76]
4	$N_2^+ + N_2^* \rightarrow N_2^+ + N_2$	1.00×10^{-9}	[76]
5	$N^+ + N \rightarrow N^+ + N$	1.00×10^{-9}	[76]
6	$N^+ + N^* \rightarrow N^+ + N$	1.00×10^{-9}	[76]
7	$N^+ + N_2 \rightarrow N^+ + N_2$	1.00×10^{-9}	[76]
8	$N^+ + N_2^* \rightarrow N^+ + N_2$	1.00×10^{-9}	[76]
9	$H_3^+ + NH_3 \rightarrow NH_4^+ + H_2$	4.40×10^{-9}	[76]
10	$H_2^+ + NH \rightarrow NH^+ + H_2$	5.00×10^{-10}	[76]
11	$H_2^+ + NH \rightarrow NH_2^+ + H$	5.00×10^{-11}	[76]
12	$H_2^+ + NH_2 \rightarrow NH_2^+ + H_2$	5.00×10^{-10}	[76]
13	$H_2^+ + NH_2 \rightarrow NH_3^+ + H$	5.00×10^{-11}	[76]
14	$H_2^+ + NH_3 \rightarrow NH_3^+ + H_2$	5.70×10^{-9}	[76]
15	$H_2^+ + NH_3 \rightarrow NH_4^+ + H$	5.00×10^{-11}	[76]
16	$H^+ + NH_3 \rightarrow NH_3^+ + H$	5.00×10^{-11}	[76]
17	$H^+ + NH_2 \rightarrow NH_2^+ + H$	5.00×10^{-11}	[76]
18	$H^+ + NH \rightarrow NH^+ + H$	5.00×10^{-11}	[76]
19	$NH^+ + NH_3 \rightarrow NH^+ + NH$	2.40×10^{-9}	[76]
20	$NH^+ + NH_3 \rightarrow NH_4^+ + N$	1.80×10^{-9}	[76]
21	$NH^+ + H_2 \rightarrow NH_2^+ + H$	1.00×10^{-9}	[76]
22	$NH_2^+ + NH_3 \rightarrow NH_3^+ + NH_2$	2.20×10^{-9}	[76]
23	$NH_2^+ + NH_3 \rightarrow NH_4^+ + NH$	2.20×10^{-9}	[76]
24	$NH_2^+ + H_2 \rightarrow NH_3^+ + H$	1.00×10^{-9}	[76]
25	$NH_3^+ + NH_3 \rightarrow NH_4^+ + NH_2$	2.20×10^{-9}	[76]
26	$NH_3^+ + H_2 \rightarrow NH_4^+ + H$	4.00×10^{-13}	[76]
27	$NH_3^+ + H_2 \rightarrow H_2^+ + NH_3$	$9.63\times10^{-13}(T_g/298)^{-0.25}EXP(-14.6/T_g)$	[27]
28	$NH_3^+ + NH_3 \rightarrow H^+ + NH_2 + NH_3$	$6.87\times10^{-10}(T_g/298)^{-0.17}EXP(-4.6/T_g)$	[27]
29	$NH_3^+ + H_2 \rightarrow H_2^+ + NH_2 + H$	$2.18\times10^{-09}(T_g/298)^{-0.20}EXP(-9.9/T_g)$	[27]
30	$NH_3^+ + NH_3 \rightarrow NH_2^+ + H_2 + NH_2$	$6.12\times10^{-07}(T_g/298)^{-0.44}EXP(-3.8/T_g)$	[27]
31	$NH_3^+ + H_2 \rightarrow H^+ + NH_3 + H$	$8.46\times10^{-10}(T_g/298)^{-0.39}EXP(-14.8/T_g)$	[27]
32	$NH_2^+ + CH_4 \rightarrow NH_3^+ + CH_3$	1.60×10^{-9}	[66]
33	$NH_3^+ + C_2H_2 \rightarrow NH_4^+ + C_2H_3$	5.40×10^{-10}	[66]
34	$NH_2^+ + CH_4 \rightarrow NH_3^+ + CH_3$	9.20×10^{-10}	[66]
35	$NH_3^+ + C_2H_2 \rightarrow NH_4^+ + C_2H_3$	1.40×10^{-9}	[66]
36	$CH_4^+ + NH_3 \rightarrow NH_3^+ + CH_4$	1.60×10^{-9}	[66]
37	$CH_4^+ + NH_3 \rightarrow NH_4^+ + CH_3$	1.46×10^{-9}	[66]
38	$CH_5^+ + NH_3 \rightarrow NH_4^+ + CH_4$	2.30×10^{-9}	[66]
39	$C_2H_4^+ + NH_3 \rightarrow NH_3^+ + C_2H_4$	2.00×10^{-10}	[66]
40	$C_2H_5^+ + NH_3 \rightarrow NH_4^+ + C_2H_4$	2.18×10^{-9}	[66]

41	$C_2H_6^+ + NH_3 \rightarrow NH_3^+ + C_2H_6$	6.60×10^{-10}	[66]
42	$C_2H_6^+ + NH_3 \rightarrow NH_4^+ + C_2H_5$	1.30×10^{-9}	[66]
43	$H_2^+ + CN \rightarrow HCN^+ + H$	1.20×10^{-9}	[66]
44	$H_2^+ + HCN \rightarrow HCN^+ + H_2$	2.70×10^{-9}	[66]
45	$H_3^+ + CN \rightarrow HCN^+ + H_2$	2.00×10^{-9}	[66]
46	$N^+ + CH_4 \rightarrow HCN^+ + H_2 + H$	5.60×10^{-11}	[66]
47	$N_2^+ + CH_4 \rightarrow CH_3^+ + N_2 + H$	9.30×10^{-10}	[66]
48	$N_2^+ + HCN \rightarrow HCN^+ + N_2$	3.90×10^{-10}	[66]

Table 14. Extra neutral-neutral reactions taken into account when ammonia is included as dilution gas. The rate coefficients are calculated by $k=k_0\times(T_g/298)^n\times\exp(-E_a/RT_g)$, where T_g is the gas temperature (K). The parameters k_0, n, and E_a are given in the table, as well as the reference where these data are adopted from.

No.	Reactions	Rate coefficient			Ref.
		$k_0(cm^3s^{-1})$	n	$E_a/R(K)$	
1	$N_2 + N_2 \rightarrow N + N + N_2$	4.29×10^{-10}	0	86460	[77]
2	$NH_3 + H \rightarrow H_2 + NH_2$	1.34×10^{-10}	0	7325	[78]
3	$NH_3 + NH + M \rightarrow N_2H_4 + M$	5.00×10^{-35}	0	0	[79]
4	$NH_2 + H \rightarrow H_2 + NH$	4.81×10^{-12}	0	0	[80]
5	$NH_2 + H_2 \rightarrow H + NH_3$	2.09×10^{-12}	0	4277	[81]
6	$NH_2 + NH_2 \rightarrow H_2 + N_2H_2$	8.31×10^{-11}	0	0	[82]
7	$NH_2 + NH_2 \rightarrow NH_3 + NH$	8.31×10^{-11}	0	5100	[83]
8	$NH_2 + N \rightarrow N_2 + H + H$	1.20×10^{-10}	0	0	[81]
9	$NH_2 + NH \rightarrow H + N_2H_2$	2.49×10^{-9}	-0.50	0	[81]
10	$NH_2 + NH \rightarrow N_2H_3$	1.16×10^{-10}	0	0	[84]
11	$NH + N \rightarrow N_2 + H$	2.50×10^{-11}	0	0	[76]
12	$NH_2 + NH + M \rightarrow NH_3 + M$	6.06×10^{-30}	0	0	[79]
13	$NH + H \rightarrow H_2 + N$	5.98×10^{-11}	0	166	[81]
14	$NH + H_2 \rightarrow H + NH_2$	5.96×10^{-11}	0	7782	[79]
15	$NH + NH \rightarrow N_2 + H + H$	1.16×10^{-9}	0	0	[85]
16	$NH + NH \rightarrow N_2H_2$	3.49×10^{-12}	0	0	[86]
17	$NH + NH \rightarrow NH_2 + N$	1.40×10^{-14}	2.89	-1015	[87]
18	$N + H_2 \rightarrow NH + H$	2.66×10^{-10}	0	12609	[88]
19	$H + H + NH_3 \rightarrow H_2 + NH_3$	1.40×10^{-31}	0	0	[89]
20	$H + H + NH_2 \rightarrow H_2 + NH_2$	1.40×10^{-31}	0	0	[89]
21	$N + H + NH_3 \rightarrow NH + NH_3$	5.00×10^{-32}	0	0	[81]
22	$H + N + H \rightarrow H + NH$	5.00×10^{-32}	0	0	[81]
23	$H + NH_2 + NH_3 \rightarrow NH_3 + NH_3$	6.00×10^{-30}	0	0	[81]
24	$N + H + H \rightarrow NH + H$	5.00×10^{-32}	0	0	[81]
25	$H + NH_2 + H \rightarrow NH_3 + H$	6.00×10^{-30}	0	0	[81]
26	$H + NH_2 + NH_2 \rightarrow NH_3 + NH_2$	6.00×10^{-30}	0	0	[81]
27	$N_2H_2 + H \rightarrow N_2 + H + H_2$	4.53×10^{-13}	2.63	-115	[89]
28	$N_2H_2 + NH_2 \rightarrow N_2 + H + NH_3$	1.53×10^{-15}	4.05	-810.7	[90]
29	$N_2H_3 + H \rightarrow NH_2 + NH_2$	2.66×10^{-12}	0	0	[91]
30	$N_2H_3 + N_2H_3 \rightarrow NH_3 + NH_3 + N_2$	5.00×10^{-12}	0	0	[92]
31	$N_2H_3 + N_2H_3 \rightarrow N_2H_4 + N_2H_2$	2.00×10^{-11}	0	0	[93]
32	$N_2H_4 + N \rightarrow NH_2 + N_2H_2$	1.25×10^{-13}	0	0	[91]
33	$N_2H_4 + H \rightarrow N_2H_3 + H_2$	1.17×10^{-13}	0	1260.5	[94]
34	$N_2H_4 + NH_2 \rightarrow NH_3 + N_2H_3$	5.15×10^{-13}	0	0	[91]
35	$N_2H_2 + H \rightarrow N_2H + H_2$	8.31×10^{-11}	0	510	[79]
36	$N_2H_2 + NH \rightarrow N_2H + NH_2$	1.66×10^{-11}	0	510	[79]
37	$N_2H_2 + NH_2 \rightarrow N_2H + NH_3$	1.66×10^{-11}	0	510	[79]
38	$N_2H + H \rightarrow N_2 + H_2$	6.64×10^{-11}	0	1531	[79]
39	$N_2H + NH \rightarrow N_2 + NH_2$	8.31×10^{-11}	0	0	[79]

40	$N_2H + NH_2 \rightarrow N_2 + NH_3$	8.31×10^{-11}	0	0	[79]
41	$N_2^* + N_2 \rightarrow N_2 + N_2$	1.90×10^{-13}	0	0	[95]
42	$N_2^* + N \rightarrow N + N_2$	1.00×10^{-13}	0	0	[95]
43	$N_2^* + N^* \rightarrow N + N_2$	1.00×10^{-13}	0	0	[95]
44	$N^* + N_2 \rightarrow N + N_2$	2.00×10^{-14}	0	0	[95]
45	$N^* + N + M \rightarrow N_2^* + M$	2.00×10^{-32}	0	0	[95]
46	$N + N + M \rightarrow N_2^* + M$	1.00×10^{-32}	0	0	[95]
47	$N + N + M \rightarrow N_2 + M$	1.00×10^{-32}	0	0	[95]
48	$N_2^* + N_2 \rightarrow N_2 + N_2^*$	1.36×10^{-09}	0	0	[95]
48	$H + H + N_2 \rightarrow H_2 + N_2$	9.11×10^{-33}	-1.32	0	[95]
49	$CH_4 + N_2^* \rightarrow CH_3 + H + N_2$	1.50×10^{-12}	0	0	[96, 97]
50	$CH_3 + N_2^* \rightarrow CH_2 + H + N_2$	4.50×10^{-11}	0	0	[96, 97]
51	$CH_2 + N_2^* \rightarrow CH + H + N_2$	3.80×10^{-13}	0	0	[96, 97]
52	$CH + N_2^* \rightarrow C + H + N_2$	1.50×10^{-12}	0	0	[96, 97]
53	$C_2H_6 + N_2^* \rightarrow C_2H_5 + H + N_2$	3.60×10^{-12}	0	0	[96, 97]
54	$CH_4 + N^* \rightarrow CH_3 + NH$	1.50×10^{-12}	0	0	[96, 97]
55	$CH_3 + N \rightarrow HCN + H_2$	1.40×10^{-11}	0	0	[96, 97]
56	$CH_3 + N \rightarrow H_2CN + H$	1.30×10^{-10}	0	0	[96, 97]
57	$CH_2 + N \rightarrow HCN + H$	8.30×10^{-11}	0	0	[96, 97]
58	$CH_2 + N \rightarrow CN + H_2$	1.60×10^{-11}	0	0	[96, 97]
59	$CH + N \rightarrow CN + H$	2.10×10^{-11}	0	0	[96, 97]
60	$CH_4 + CN \rightarrow HCN + CH_3$	7.00×10^{-13}	2.30	16.0	[96, 97]
61	$H_2CN + N \rightarrow HCN + NH$	6.70×10^{-10}	0	0	[96, 97]
62	$CN + H_2 \rightarrow HCN + H$	4.80×10^{-13}	2.60	-960.0	[96, 97]
63	$N + C_2H_4 \rightarrow HCN + CH_3$	1.66×10^{-14}	0	0	[96, 97]
64	$C_2H_6 + CN \rightarrow HCN + C_2H_5$	1.79×10^{-12}	2.70	-810	[96, 97]
65	$C_2H_4 + CN \rightarrow HCN + C_2H_3$	2.09×10^{-10}	0	0	[96, 97]
66	$CH_3 + H + N_2 \rightarrow CH_4 + N_2$	6.00×10^{-29}	-1.80	0	[96, 97]
67	$C_2H_2 + H + N_2 \rightarrow C_2H_3 + N_2$	1.08×10^{-25}	-7.27	3623	[96, 97]

Table 15. Sticking coefficients used in the model for all the radicals

Species	Sticking coefficient	Reference	Species	Sticking coefficient	Reference
H	0.01	[98]	C_6H	0.80	[99]
C	1.00	[99]	C_6H_3	0.30	[99]
CH	1.00	[99]	C_8H	0.80	[99]
CH_2	0.26	[99]	$C_{10}H$	0.80	[99]
CH_3	0.001	[99]	$C_{12}H$	0.80	[99]
C_2	1.00	[99]	CN	0.85	[100]
C_2H	0.80	[99]	N	0.005	[81]
C_2H_3	0.30	[99]	NH	0.11	[100]
C_2H_5	0.01	[99]	NH_2	0.6	[100]
C_4H	0.80	[99]	N_2H	0.14	[81]
C_4H_3	0.30	[99]	N_2H_3	0.05	[81]

Table 16. Decomposition rate (DR) of the background gas molecules, calculated for the four different gas mixtures and two pressure values under study. The negative values mean that more background gas species are formed instead of decomposed.

	DR	50mTorr	1Torr
CH_4/H_2	CH_4	49.62%	2.92%
	H_2	8.74%	0.20%
CH_4/NH_3	CH_4	75.14%	71.87%
	NH_3	89.92%	89.50%
C_2H_2/H_2	C_2H_2	85.40%	69.59%
	H_2	-7.93%	-16.27%
C_2H_2/NH_3	C_2H_2	84.76%	96.09%
	NH_3	83.59%	97.02%